Characterization and doping of photochromic $BaMgSiO_4$ with 1st row transition metals and lanthanides

University of Turku

Faculty of Science

Department of Chemistry

Intelligent Materials Chemistry Research Group

Master's thesis

Author:

Araz Osmanov

05.05.2025

Master's thesis

Subject: Materials Chemistry

Author(s): Araz Osmanov

Title: Characterization and doping of photochromic $BaMgSiO_4$ with 1st row transition metals and lanthanides

Supervisor(s): Prof. Mika Lastusaari, Adj. Prof. Anssi Peuronen, Minnea Tuomisto (postdoctoral researcher)

Number of pages: 70

Date: 05.05.2025

In recent years, there has been an increased focus on the study of tunable inorganic luminescent and photochromic(color-changing) materials. Most of the silicates have poor photochromic properties. However, by doping these particles with specific dopants, these properties can be enhanced. $BaMgSiO_4$ (Barium Magnesium ortho-silicate, shortly BMS) is a member of the silicate salts that are suitable for enhancing photochromism using various dopants. Inorganic photochromics provide exceptional heat stability and chemical resistance, making them highly promising for use in multiple applications.

The aim of this work is to synthesize radiation-responsive materials and dope them with various transition metals and lanthanides. Testing these dopants on photochromic BMS materials helps to determine their suitability for dose-quantification analyses within the X-ray and UV range.

Several first-row transition metals (Fe, Cr, Co, Zn, Cu, V, Ni, and Mn) and a few lanthanides (Eu and Dy) were tested under two different reaction conditions (air and N_2/H_2) with photochromic BMS samples. The results revealed that the N_2/H_2 atmosphere is the most effective reaction condition for synthesis.

After selecting the optimal condition, the dopant concentrations were varied—standard (0.05%), halved (0.025%), and doubled (0.1%)—to determine the optimal concentration for each dopant. Further testing confirmed that the synthesized materials are suitable for UV and X-ray radiation detection analyses.

Key words: dopant, silicates, luminescence, photochromism, UV, X-Ray

Table of Contents

Abbreviations

BMS – Barium Magnesium Silicate

EPR- Electron Paramagnetic Resonance

PeL – Persistent Luminescence

RS – Reflectance Spectroscopy

LS – Luminescence Spectroscopy

LED – Light Emitting Diode

SSL – Solid-State Lighting

ODS – Optical Data Storage

TL – Thermoluminescence

XRD – X-ray Powder Diffraction

XRF – X-ray Fluorescence

1. INTRODUCTION

The process of an excited electron traveling from a higher energy orbital to a lower one, producing emission of light, is known as luminescence. Photochromism is a reversible color change by exposure to light on the materials. A large number of luminescent and photochromic materials have extensive uses globally, based on different areas such as information displays, lighting, X-ray intensification, scintillation, LEDs, dosimetry, etc. [1-3]. Specifically, in phosphor science, certain inorganic silicates are key to luminescence, and consequently, studies on inorganic luminescent and photochromic materials with variable properties have aroused reasonably wide attention. Based on the excitation source, luminescence can exist in numerous forms. Some materials show photoluminescence, which is light emission caused by photons. Some others show thermoluminescence, which is a type of light emission that happens when certain crystals, like some minerals, release stored energy as light when they are heated. There is also cathodoluminescence, which happens when an electron beam causes the material to emit light. Photochromism and photoluminescence will be discussed in this project through various studies, which will be detailed in the following chapters.

1.1. Principles and applications of photochromic materials

Photochromism is the effect observed in photochromic materials, in which color modification is induced due to exposure to light [5]. Materials that respond by reversibly changing color upon exposure to external stimuli have gained significant interest due to their technological applications in areas such as sensors, energy, decoration, bio-imaging, and catalysis, among others. Typically, the color change is the result of a broad range of stimuli, including thermal changes, mechanical stress, light, electrical input, magnetic fields, and nuclear radiation [6]. Photochromism may also be defined as the reversible change of a compound between two states: a stable state (before irradiation) and a metastable state, which is caused by irradiation [6].

Photochromic systems are of growing interest due to their applications in ophthalmic lenses and as smart molecular materials capable of acting as photoresponsive self-assembling systems, molecular switches, logic gates, and information storage media [7].

The photochromism term can also be understood in terms of photoisomerization. It relies on the reversible process by which a molecule is transformed from one isomer to another when exposed to light. The isomers possess distinctly different absorption spectra, i.e., they absorb differently at different wavelengths. Photoisomerization is often found in molecules like certain pigments or chemicals used in light-sensitive materials. Reversible photoisomerization by light can cause physical property changes in photochromic compounds. These alterations may be changes in properties such as absorption spectra, fluorescence emission, conjugation, conductivity of electrons, electrochemical properties, magnetic properties, coordination properties, dipole interactions, refractive index, dielectric constant, and even the geometry of the molecule. This feature has inspired the use of photochromic compounds as photochemical molecular switches. Molecular switches are simply units that may switch between two distinct physical forms, typically based on stimuli from light, electricity, or chemicals. Molecular switches are critical constituents in a broad range of optoelectronic devices and useful materials. The physical properties of the materials can be controlled and manipulated when they are activated by their respective stimuli [8].

Photochromic materials have gained quite wide interest for multi-photon devices [10],[11], surface and nanoparticle technologies [12], photo-electronic devices [13], and electrochemical wiring [14], among others. Their ability to reversibly switch properties with light opens up many possibilities for advanced technology and innovative materials [9].

1.2. Principles and applications of photoluminescent materials

When a material absorbs a photon (in the UV range), one of its electrons is excited to a higher electronic excited state. When the electron drops to a lower level of energy, the molecule emits a photon (in the visible range). This is what is called photoluminescence. The photon emitted has a longer wavelength (i.e., lower energy) than the photon absorbed if the molecule redistributes internal energy following the primary photon absorption. There are different types of photoluminescence, such as fluorescence and phosphorescence, which happen when an electron moves to a state with a different spin (called a higher spin multiplicity) through a process known as intersystem crossing [15].

Active center and active medium of luminescent materials are essential requirements to be viewed or achieved to obtain effective luminescence. Energy radiations in the forms of X-rays, CRT, or UV radiation from the excitation source can be altered by luminescent materials into visible light or infrared radiation.

Luminescent materials can be generalized into three groups according to their performance: (i) host luminophore, (ii) host and activator, and (iii) host and sensitizer +activator.
The host luminophore is made up of active centers that absorb the energy of excitation and emit radiation. The host and activator constitute an inactive host containing luminescent active centers. In the sensitizer + activator and host system, an excitation energy is taken up by a sensitizer and passed to the activators within the host in order to enhance the material's luminescent properties. [16] Photoluminescent materials are employed mostly in light-emitting diodes (LEDs) and additionally in plasma and vacuum fluorescent displays. These materials are generally doped with rare earth (RE) elements, which have a broad energy level range, and hence emissions occur over a wide range of colors [16].

White LEDs are recognized as better alternatives to halogen, xenon, and incandescent lamps owing to their high luminous efficiency, longer life, excellent light stability, and eco-friendliness [16]. In addition to their use in solid-state lighting (SSL), light-emitting diodes (LEDs), and display devices, luminescent materials with superior luminescence properties have broad applications in solar cells, sensors, and biomedical sciences. Their multi-functionality has encouraged researchers to seek new and improved materials with superior luminescent properties. Rare earth (RE) ions, because of their ladder-like energy structure and sharp emission lines, have a major impact on this field [17].

Thermoluminescence (TL) dosimetry has developed over the last half-century through successful practice. Personal dosimetry and environmental monitoring are among its most frequent applications. TL dosimetry has found widespread applications in medical physics today, including radiation therapy, diagnostic radiology, and nuclear medicine. High-temperature high-dose measurement and retrospective dosimetry are topics of interest at present [18].

Photon energy storage and photochromic conversion open up a great range of future applications in fields of high-density optical data storage (ODS), photoswitching, anti-counterfeiting, and imaging in biology. Photon storage based on photochromic materials has come a long way, showing sufficient superiority compared to conventional 2D optical storage media

such as CDs, by offering better three-dimensional spatial resolution, shorter information access time, as well as multiplexed storage capability [19]. The principle is based on the reversible coloration and bleaching state of photochromic compounds for recording binary data ("0" and "1") according to photon excitation at different wavelengths. For practical applications in future 3D optical memory devices, photochromic compounds as recording media are required to enable effective writing, erasing, and reading processes. In essence, appropriate photochromic materials for environmentally friendly optical storage devices must satisfy fundamental requirements, such as effective luminescence for reading data, high response speeds, and effective resistance. Most importantly, control over luminescence intensity provides a highly efficient means of reading stored data as it increases detection sensitivity and decreases signal interference [19].

1.3. Photochromism and luminescence in $BaMgSiO_4$

$BaMgSiO_4$ (BMS) is a material with widespread prospects for use in photochromics based on its optoelectronic and non-linear optical properties. Since BMS is such a material with application areas from high-density optical storage to switchable windows, photo switches, and LEDs, scientists across the world are highly interested in it [20]. In WO_3 materials, visible-light photochromism is usually accompanied by water decomposition, and it even finds application in solar energy conversion [21]. BMS is an extremely good host material for doping in order to make it stable and to exhibit color-changing properties. It contains a unit cell volume of 0.6306 nm^3, lattice parameters a = 0.91226 nm, c = 0.87496 nm, which follows a stuffed tridymite structure with space group $P6_3$ [22].

BMS is formed by corner sharing with MgO_4 and SiO_4 tetrahedra. There are four different sites in the structure, and each one is bonded to Ba^{2+}, Mg^{2+}, and Si^{4+} with different coordination shapes. Tridymite structure (Figure 1) [22],[23] is formed by corner-linking these tetrahedra. Doped with Europium (Eu), it confers BMS with long-duration luminescence, which is appropriate for a range of uses such as bioimaging, glow-in-the-dark products, and emergency signs [20].

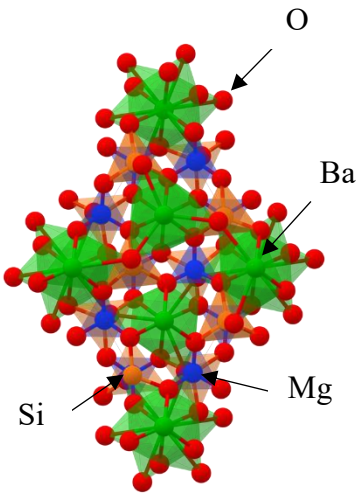

Figure 1. The crystal cage of $BaMgSiO_4$ [23].

Photochromism is initiated by doping BMS with different dopants. The doping process is regulated by the ionic radii of the dopant and the material to be doped [24]. When, for instance, BMS is doped with Eu^{3+}, Eu^{3+} ions substitute Ba^{2+} ions of the crystal lattice. It is facilitated by electron transfer interaction between the dopant Eu ions and lattice oxygen vacancies [25].

In order to irradiate Eu^3-containing samples, high-energy rays like UV light, X-rays, γ-rays, or ultrafast femtosecond lasers are usually employed. Nevertheless, this approach is only suitable for a limited number of special compounds possessing rigid three-dimensional enclosed crystal structures, such as sulfates ($BaSO_4$:Eu), phosphates ($Ba_3(PO_4)_2$:Eu), borophosphates ($MBPO_5$:Eu, where M = Ca, Sr, Ba), borates (e.g., SrB_4O_7:Eu, SrB_6O_{10}:Eu, $Sr_2B_5O_9Cl$: Eu, BaB_8O_{13}:Eu), aluminates ($Sr_4Al_{14}O_{25}$:Eu), and silicates ($MAl_2Si_2O_8$:Eu). These compounds have gained attention in research and applied chemistry because they are cost-effective, safe, and easy to prepare [26].

Synthesizing photochromic compounds with reversible luminescence usually involves complicated chemical synthesis with many time-consuming purifications, so efficient solutions have been an area of interest as a result. More resilient to heat, wear, and chemicals than organic photochromic compounds, inorganic compounds have been investigated over the past few decades for optical information storage. Materials such as MoO_3, TiO_2, WO_3, $SrTiO_3$, Sr_2SnO_4, $BaMgSiO_4$, and $Bi_{2.5}Na_{0.5}Nb_2O_9$ have been of interest. One such interesting compound is $BaMgSiO_4$:Eu^{2+}

(BMS:Eu), which possesses superior reversibility, is a quick responder (takes only a matter of seconds), and features bright pink switching of colors. Altogether, it is an apt choice for applications such as permanent phosphors and white LEDs. Unfortunately, little study has been made of its 3D optical storing promise, with modulation of luminescence, which would be revolutionary [27].

1.4. Photochromic dosimeters and dose quantification

Light dosimeters are extensively used to precisely measure cumulative radiation doses, thereby preventing excessive exposure [28-30]. With photochromic dosimeters, both qualitative and quantitative X-ray dose measurements can be achieved through colorimetric analysis and absorption spectroscopy [31],[32]. The photochromic behavior is attributed to the trapping and detrapping of charge carriers at oxygen vacancies, as evidenced by the results obtained from in situ EPR measurements for BMS. The photochromic transition from white to pink helps to understand dosimetry quantification analysis of X-ray and UV light, while the reverse bleaching process from pink to white presents potential for reusable or resettable dosimetric applications [3].

X-ray-induced photochromism has attracted widespread interest at present on the basis of its versatility in being applied in diversified areas [6]. X-ray-sensitive materials are usually required with electronic equipment or multi-step processes to search for traces of X-rays [33-35]. It would, however, significantly simplify the work to directly visualize X-rays through color change and make it very convenient, as the equipment required would be very minimal, so that it could directly give corresponding information if required [36]. Photochromic dosimeters are extremely convenient for inclusion in smart devices for cumulative X-ray dose measurement, particularly since this reversible visual technique eliminates the need for proportional counters, ionization chambers, semiconductor detectors, scintillators, imaging systems, or other expensive instruments that require skilled operators [3],[37].

1.5. Mechanism of Photochromism in BMS

F-center formations are typically described as turning points for reversible photochromism [38]. Its designation "F-center" is derived from the German term for "Farbe," which means "color," since it is accountable for color in material. An F-center is a point crystallographic defect resulting from an anion site occupied by one or more unpaired electrons [39]. Optical absorption by such compounds is attributed to electron transitions between energy levels of defects in the visible light range, which is responsible for creating the appearance of color. Further, the dynamic electron trapping process followed by release at F-centers emphasizes mechanisms of coloration and bleaching, respectively [6].

Yang et al confirmed that oxygen vacancies were the responsible principle in forming F-centers by in-situ electron paramagnetic measurements (EPR). From measurement, it was noted that under reducing atmosphere condition (N_2/H_2), there were more oxygen vacancies formed in synthesizing the sample [3].

1.6. Conclusion and Aims of the Project

This study will seek to synthesize photochromic BMS, add dopants made up of transition metals and some selected lanthanides, and study their photochromic behavior at various scales. It will be shown that BMS can be doped using diverse methodologies, leading to some changes in its optical properties, consequently opening up a broad range of possible industrial applications. This change can be enhanced by manipulating the precursor material used, i.e., the transition metal dopant material. Some experimental studies were carried out to study photochromism by BMS. Some of the main aims of this study involve improving the photochromic properties of BMS with the addition of transition metals and lanthanides. Appropriate dopants based on 1^{st} row transition metals and lanthanides, dopant concentration levels, and effects caused by reaction conditions on samples in terms of assessing their photochromic properties were evaluated in this study.

2. EXPERIMENTAL

Materials characterization is fundamental in experimental work to determine the composition and key properties of synthesized samples. For the BMS-doped samples in this study, multiple analytical techniques to systematically investigate their structural, photochromic, and luminescent characteristics were used. The characterization approach was designed to provide comprehensive insights into the material's behavior under different conditions.

2.1. Sample preparation

$BaMgSiO_4$:X samples were synthesized *(reaction 1)* following the protocol reported by *Akiyama et al*.[22].

$2BaCO_3(s) + 2MgCO_3(s) + 2SiO_2(s) \xrightarrow{1170^{o}} 2BaMgSiO_{4(s)} + 4CO_{2\,(g)}$ *(reaction 1)*

In mortar, those materials were ground with 2-3 drops of ethanol and put into the furnace at 75°C for preheating to get rid of ethanol.

The reactions consist of three sets: 1) Standard amount of dopants (0.05%-mass) 2) doubled amount of dopants (0.1%-mass); 3) halved amount of dopants (0.025%-mass). The amounts of materials were calculated due to their stoichiometric coefficients (Table 1).

Table 1. Amounts of materials for experiments.

Source materials	***Amounts (in g)***
$BaCO_3$ (Pro analysi, Merck 99%)	1.1
$MgCO_3$ (Pro analysi, Merck 99%)	0.52
SiO_2 (fumed, Sigma Aldrich, 99.8%)	0.3
H_3BO_3 (as flux, (J.T. Baker, 99.5%)	0.1
Source of dopants TiO_2 – Aldrich 99.8% V_2O_5 – Aldrich >98% Cr_2O_3 – Sigma Aldrich >98% MnO – Aldrich 99% Fe_2O_3 – EMSURE 99.8% CoO – Merck Darmstadt 98% CuO – E-Merck Darmstadt 98% $NiCl_2$ – Aldrich 99.9% ZnO – EMSURE 99.8%, Dy_2O_3 – International Laboratory USA 99.9% Eu_2O_3 – International Laboratory USA 99.9%	0.001(mass-0.05%) 0.0005(mass- 0.025%) 0.002(mass-0.1%)

The initial set of reactions was conducted to evaluate photochromism using various dopants and determine which ones are effective for the study's objective. Following the reactions, Mn, Cr, Co, and Fe were selected as essential dopants.

Then the mixtures of these materials were transferred to an aluminum oxide reaction vessel and put into Lenton oven at 1170°C for 4 hours with the heating and cooling rate of 20°C/min air and reducing atmosphere (12% H_2 and 88% N_2) conditions.

Synthesized samples: $BaMgSiO_4$:X (X- Ti, V, Cr, Mn, Fe, Co, Cu, Ni, Zn, Dy, Eu)

Once the reaction finished, the reaction vessels were taken out of the oven and cooled down to room temperature. After completing synthesis, the samples were extracted from the vessel and were powdered.

2.2. Characterization

Following the synthesis process, the elemental and phase compositions of the products were characterized using powder X-ray diffraction (XRD) and X-ray fluorescence spectroscopy (XRF). For testing photochromism and luminescence processes, reflectance spectroscopy and luminescence spectroscopy analyses were conducted. For investigating a potential application of BMS, X-Ray and UV-dosimetry were tested.

2.2.1. X-Ray Fluorescence (XRF)

X-ray fluorescence spectroscopy was employed to determine the elemental composition of the sample and its corresponding concentrations (% and ppm). The instrument - PANalytical Epsilon 1 featured an internal Omnian calibration, a 50 kV silver-anode X-ray tube with Kα emission around 22 keV, and an SDD5 detector. The powdered sample was positioned in a holder with a transparent film covering its base and then placed in the instrument's sample chamber for a measurement lasting 1 hour.

2.2.2. X-Ray Powder Diffraction (XRD)

XRD patterns were recorded on a PANalytical Aeris powder X-ray diffractometer operating at 40.0 kV and 7.5 mA with a PIXcel1D-Medipix3 detector and Cu-$K_{\alpha 1,\alpha 2}$ radiation (λ = 1.5406 Å, 1.5444 Å). The following optical and data collection parameters were employed: nickel beta-filter, 0.04 rad soller slits, 1/4° divergence slit, 13 mm fixed mask, high beam knife, 9 mm anti-scatter slit, 1 rps spinner speed, 0.201 °/s scan rate and 0.0217° step size. XRD patterns were treated using HighScore software with the ICDD PDF-4+ database. Background was computed with a bending factor of 2 and granularity of 20 using smoothed input data. Peaks of minimum significance: 3.00, minimum tip width: 0.01, maximum tip width: 1.00, peak base width: 2.00 were calculated by the minimum 2nd derivative method and referenced to a pattern list contained in the ICDD PDF-4+ database.

2.2.3. Reflectance Spectroscopy (RS)

Reflectance spectra of the samples were measured to find out their light absorption properties. The photochromic properties of samples were defined by reflectance spectrum after five-minute irradiation under UV at 254, 302, and 365 nm wavelengths. Konica Minolta CM-2300d was used as the measuring instrument. It has dark and white references, but no specific names by itself. After calibrating the Konica instrument, the materials were analyzed, and the data were plotted. The measurements with Konica Minolta were done with minimal ambient lighting (in a dark room).

2.2.4. Luminescence Spectroscopy (LS)

Luminescence spectra were recorded on the Varian Cary Eclipse spectrometer. The excitation and emission spectra of all the samples were scanned under phosphorescence mode with a delay time of phosphorescence 0.0051 seconds. To recognize the peak of maximum emission, excitation wavelengths at 254, 302, and 365 nm were employed in a wavelength range of 300–900 nm in recording the emission spectrum. The emission slit width was set at 5.0 nm and excitation slit width was at 20 nm during measurements. For excitation spectra measurement, the emission wavelength was adjusted at the peak position of the emission spectrum, and the range of measurement was 200–700 nm. For weaker luminescent samples, the PMT detector voltage was adjusted to 800V, and for stronger luminescent samples, it was adjusted to 600V. The long-term luminescent emission spectra of the BMS: Eu^{2+} sample were recorded in bio-/chemi luminescence mode after UV irradiation at 254, 302, and 365 nm for 5 minutes, with high voltage and a range of wavelengths from 300–900 nm.

2.2.5. X-Ray and UV exposure for analyzing photochromic behavior

To examine the photochromic behavior of doped-BMS, both X-ray exposure and UV exposure tests were conducted under different experimental setups. For UV dosimetry, the measurements were conducted on three groups of UV light: UV-A, UV-B, and UV-C. Prior to making the measurements, the light sources, including the Ocean Insight Halogen Light Source HL-2000 as the visible light source and the UV light sources, were warmed up for 30 minutes. Once the light

sources had stabilized, the dosages of the UV lights were measured with the Opystec Dr.Gröbel Radiometer RM 12 to measure the precise dosage of the UV light being emitted.

The dark reference was taken with all of the lights in the room turned off to ensure that there would be no interference from external light sources, while the white reference, an empty PTFE holder, was read under the same conditions as actual measurements. Following this, coloration dosimetry of the materials was analyzed with the assistance of an Avantes Starline AvaSpec-ULS2048CL-EVO spectrometer and 1000 μm VIS/NIR 0.37NA PC04 optical fiber and Ocean Insight Halogen HL-2000 as a white light source, for witnessing the light-induced color changes in the materials.

After the UV dosimetry analysis was completed, X-ray dosimetry tests were run. PANalytical Epsilon 1 was used as the X-ray radiation source. The samples were exposed to X-rays for one hour using the Omnian setup with a 50 kV silver-anode tube (Kα ~22 keV) and an SDD5 detector. The samples were prepared in five lots of 1 minute, two lots of 5 minutes, and three lots of 15 minutes. For tracing the color change of samples, the same experimental setup used for UV dosimetry was applied. Each sample's coloring was observed after every exposure time, and 10 readings were taken on each sample throughout the process. The readings were crucial in establishing the photochromic response of X-ray-exposed doped BMS material.

2.2.6. Optical Microscopy for Eu-0.05% doped sample

Optical microscopy was conducted on the Eu-doped sample using a Nikon SMZ800 stereo microscope with a C-W 10X/22 ocular lens to examine the sample under different illumination conditions. The sample was excited using three excitation wavelengths, i.e., 254 nm, 302 nm, and 365 nm, as well as visible light to examine its optical response. The Nikon SMZ800 microscope provided good resolution for imaging, allowing the morphology of the sample to be observed in detail under UV and visible light. Probing with different excitation wavelengths helped to identify different electronic transitions, while 254, 302, and 365 nm were employed for identifying

potential Eu^{2}-related emission. Multi-wavelength use allowed preliminary analysis of reduction progress by observing changes in color and luminescence under varying illumination.

3. RESULTS AND DISCUSSION

3.1. Effect of dopant concentrations and reaction conditions on the doped BMS samples

BMS samples doped with different concentrations of dopants were prepared to determine the most appropriate dopant for optimizing photochromism. The most promising dopants (Fe, Cr, Co, and Mn) were selected from reflectance spectroscopy measurements and were studied further to determine the optimal doping concentrations. The results are a contribution to the development of better photochromic materials for X-ray and UV applications. Synthesis in a reducing atmosphere is known to assist the material in creating oxygen vacancies, which are essential sites that create color centers [3]. The material synthesized in air is largely free from such vacancies and thus is unable to exhibit much photochromic activity.

3.1.1. X-Ray Powder Diffraction

First, samples containing first-row transition metals (Fe, Ni, Mn, Cr, Co, Cu, Zn, and V) and lanthanides (Dy and Eu) were synthesized in both air and a reducing atmosphere. Based on the results of reflectance spectroscopy, the reducing atmosphere was determined to be the optimal condition for synthesis. Further analysis was conducted using the best-performing dopants. For each sample, the most prominent phase (04-011-361) was identified using the HighScore PANalytical software.

The XRD patterns reveal that the doped $BaMgSiO_4$ crystal structure remains stable despite the various dopant concentrations. The diffraction peaks' coherence with the reference phase is a witness to the fact that the doping materials were built into the host lattice without disturbing the

phase composition. There are some minor impurities (in ppm and %) on the samples based on X-ray fluorescence measurements (see below). Nevertheless, in most cases, these impurities are not seen as separate phases in the diffraction patterns. The stability of the diffraction patterns also shows that the doped samples are crystalline, which is a requirement to provide optical and photochromic stable properties.

In the air-sintered samples, the dopant concentration was standard (0.05%). The samples are also pure, with some samples having fewer impurities that do not affect the aim of the work. Figure 2 presents the doped samples with different dopant concentrations synthesized under a reducing atmosphere.

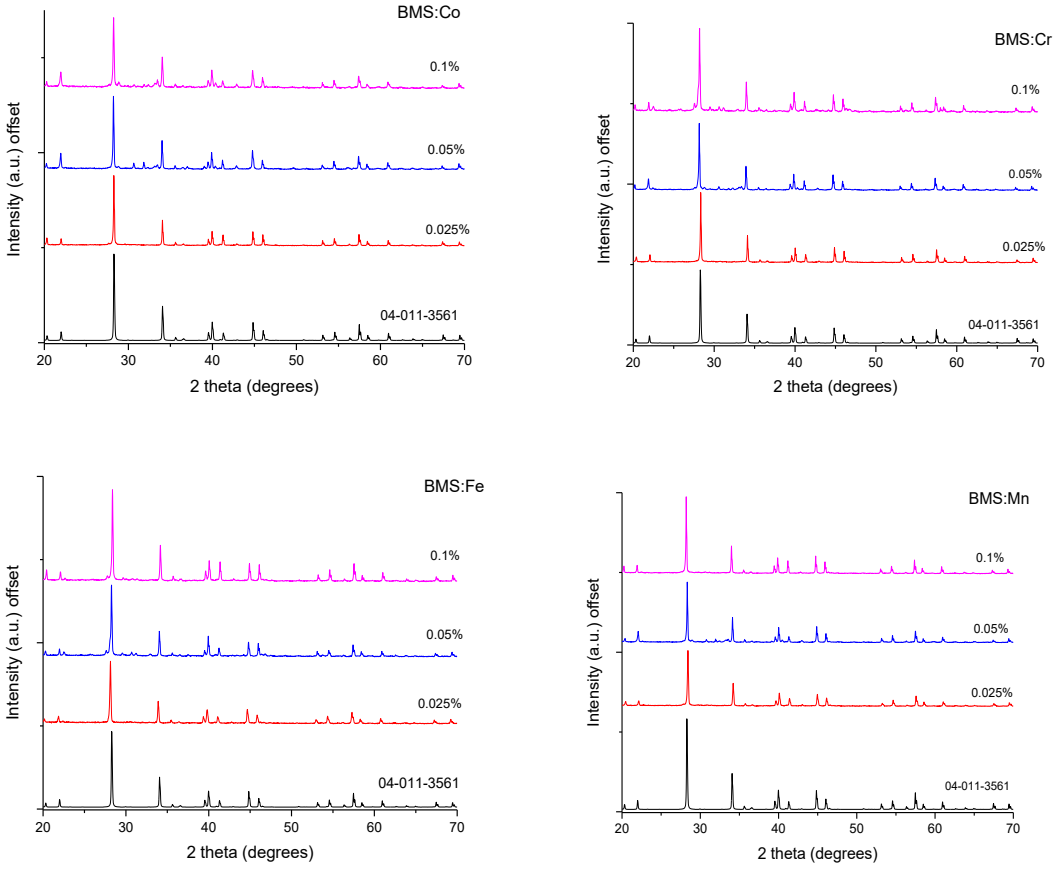

Figure 2. XRD patterns of the doped sample with different concentrations under the reducing atmosphere and the corresponding phase from the software.

The XRD patterns of the doped $BaMgSiO_4$ samples synthesized in an air environment indicate that all doped samples possessed the primary crystal structure. The presence of well-resolved peaks relating to the reference phase confirms the successful development of the phase without significant secondary phases. However, slight differences in peak intensity among different dopants can indicate that there are a few impurities in the phase, but not highly affected. These differences could be due to the difference in dopant solubility and its effect on lattice stability. The collective structural stability of the samples within the air environment is a measure of the tolerance of the material towards changing dopants without sacrificing its phase purity. (Figure 3)

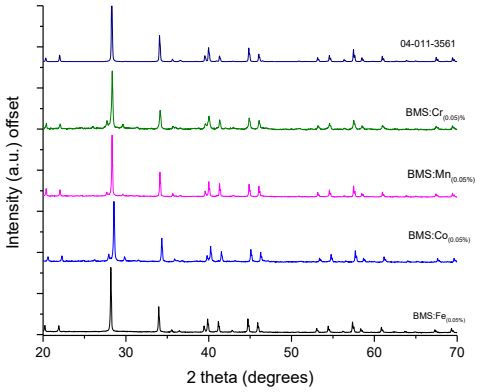

Figure 3. XRD patterns of the doped sample with the same concentrations under an air atmosphere and the corresponding phase from the software.

As mentioned before, the materials were also tested with two of the lanthanides (Eu and Dy), both in air and reducing atmosphere. But they don't have strong photochromic properties as in chosen metals. Figure 4 shows the XRD data for reducing and air atmosphere sintered lanthanide samples.

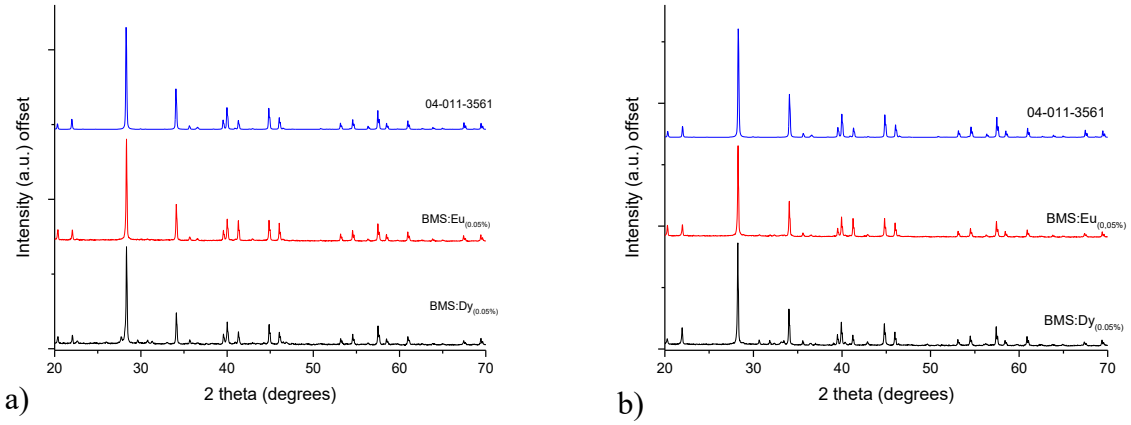

Figure 4. XRD patterns of lanthanide-doped samples: a) reducing atmosphere; b) air atmosphere.

3.1.2. X-Ray Fluorescence

XRF analyses were conducted to check the impurities of the samples by analyzing the samples' elemental composition. Tables (2-5) for XRF data represent the data from materials during the measurement, and their units are presented as ppm or %. Tables 2, 3, 4, and 5 show the XRF data for mass-0.1%, 0.05%, 0.025%, and lanthanides-0.05% samples, accordingly.

Table 2. XRF data for mass-0.1% samples.

Elements	BMS:Co	BMS:Fe	BMS:Cr	BMS:Mn
Mg	5.20 %	4.58 %	3.989 %	5.024 %
Al	0.811 %	0.0 ppm	0.0 ppm	0.607 %
Si	8.963 %	18.498 %	15.722 %	10.015 %
S	357.1 ppm	343.6 ppm	-	39.0 ppm
Cl	0.21 %	0.141 %	0.911 %	894.6 ppm
Fe	0.1 %	0.43 %	121.8 ppm	663.7 ppm
Co	0.315 %	-	-	-
Zn	162.7 ppm	-	-	0.361 %

Ga	0.156 %	-	-	-
Br	144.1 ppm	-	54.3 ppm	409.4 ppm
Sr	0.198 %	0.170 %	0.260 %	0.190 %
Sn	0.24 %	0.231 %	0.343 %	0.233 %
Ba	83.4 %	79.157 %	82.307 %	82.937 %
Eu	0.152%	0.373%	0.444 %	-

Table 3. XRF data for mass-0.025% samples.

Elements	BMS:Co	BMS:Fe	BMS:Cr	BMS:Mn
Mg	5.484 %	4.500 %	4.196 %	5.138 %
Al	0.619 %	0.6 ppm	9.0 ppm	0.885 %
Si	8.749 %	18.550 %	15.988 %	9.994 %
S	352.0 ppm	351.3 ppm	-	47.2 ppm
Cl	0.241 %	0.341 %	0.922 %	902.0 ppm
Ti	10.0 ppm	9.2 ppm	0.272 %	9.4 ppm
Fe	0.001 %	0.313 %	129.8 ppm	659.4 ppm
Co	0.456 %	-	-	-
Zn	167.5 ppm	-	-	0.504 %
Sr	0.420 %	0.465 %	0.344 %	0.047 %
Zr	1.5 ppm	7.8 ppm	16.2 ppm	13.7 ppm
Sn	0.449 %	0.471 %	0.263 %	0.332 %
Ba	83.292 %	79.299 %	82.382 %	82.710 %
Eu	0.158 %	0.426 %	0.438 %	-

Table 4. XRF data for mass-0.05% samples.

Elements	BMS:Co	BMS:Fe	BMS:Cr	BMS:Mn
Mg	5.32 %	4.71 %	4.15 %	5.18 %
Al	0.840 %	0.0 ppm	0.0 ppm	0.620 %
Si	9.12 %	18.64 %	15.95 %	10.25 %
S	368.9 ppm	347.2 ppm	43.7 ppm	42.9 ppm
Cl	0.24 %	0.152 %	0.923 %	910.8 ppm
Fe	0.14 %	0.50 %	127.4 ppm	672.9 ppm
Co	0.340 %	-	-	-
Zn	175.3 ppm	-	-	0.372 %
Sr	0.210 %	0.181 %	0.265 %	0.16 %
Sn	0.260 %	0.228 %	0.360 %	0.257 %

I	670.5 ppm	0.0 ppm	628.6 ppm	-
Ba	83.7 %	80.450 %	82.910 %	83.620 %
Eu	0.155 %	0.380 %	0.470 %	-

Table 5. XRF data for lanthanide-0.05% samples.

Elements	BMS:Dy (red. atm.)	BMS:Eu(red. atm.)	BMS:Dy (air)	BMS:Eu (air)
Mg	3.266 %	-	3.994 %	9.640 %
Al	0.489 %	1.028%	0.752 %	0.841 %
Si	8.463 %	12.82 %	8.895 %	9.693 %
S	73.1 ppm	279.3 ppm	68.9 ppm	14.8 ppm
Cl	715.3 ppm	0.311 %	859.7 ppm	0.203 %
Sr	0.183 %	0.221 %	0.181 %	0.174 %
Zr	20.8 ppm	2.7 ppm	18.1 ppm	11.4 ppm
Sn	0.213 %	0.366 %	0.224 %	0.202 %
Te	813.4 ppm	913.4 ppm	0.102 %	354.0 ppm
Ba	86.461 %	84.399 %	85.525 %	75.892 %
Eu	0.289 %	0.665 %	0.337 %	0.423 %
Dy	0.397 %	-	0.166 %	0.0 ppm

The results show that the composition of the synthesized materials, with variations in elemental concentrations, aligns with the desired doping strategies without any significant impurities. There are indeed some impurities in the samples. For example, Table 5 shows a Sc impurity exceeding 0.2% in each sample, while some samples contain Al 0-1%. Nevertheless, such impurities are present in all cases and do not significantly affect the overall composition of the samples.

3.1.3. Reflectance Spectroscopy

RS measurements were done with three different wavelengths, 254 nm, 302 nm, and 365 nm. Konika Minolta was used as a spectrometer, and SpectraMagic™ NX2 as a software. First, calibration was conducted with zero and white modes. Then, each material was tested with a before and after UV spectrum. Konika Minolta has the advantage of conducting measurements even in the light room, but in any case, the measurements were done in the dark room.

The measurements were done for each of the synthesized samples, but after deep

consideration of the results, the most effective dopants (Fe, Cr, Co, and Mn) for photochromism enhancement were chosen for further analyses. Figures below show the synthesized most essential materials' spectrum in both air and reducing atmosphere.

In the spectra, there is an absorption peak observed around 525 nm, within the green region of the spectrum, for reducing atmosphere synthesized samples. This shows that the Fe doping plays an important role in the material's light absorption, potentially influencing its photochromic behavior.

Comparing the samples synthesized in air and reducing atmospheres, slight variations in reflectance behavior can be observed. The reducing atmosphere appears to affect the intensity of the absorption feature, due to creating oxygen vacancies for color centers. These changes can influence electronic transitions, thereby modifying the optical response of the material.

In the case of Fe-doped samples with 0.1% and 0.025% concentrations, a more pronounced difference in reflectance is obvious. A stronger absorption band in the visible region suggests a higher degree of light interaction, which could impact the material's potential for optical applications. The blue-shift or red-shift in absorption features across samples further shows that compositional variations alter the electronic structure and optical properties of the material (Fig.5).

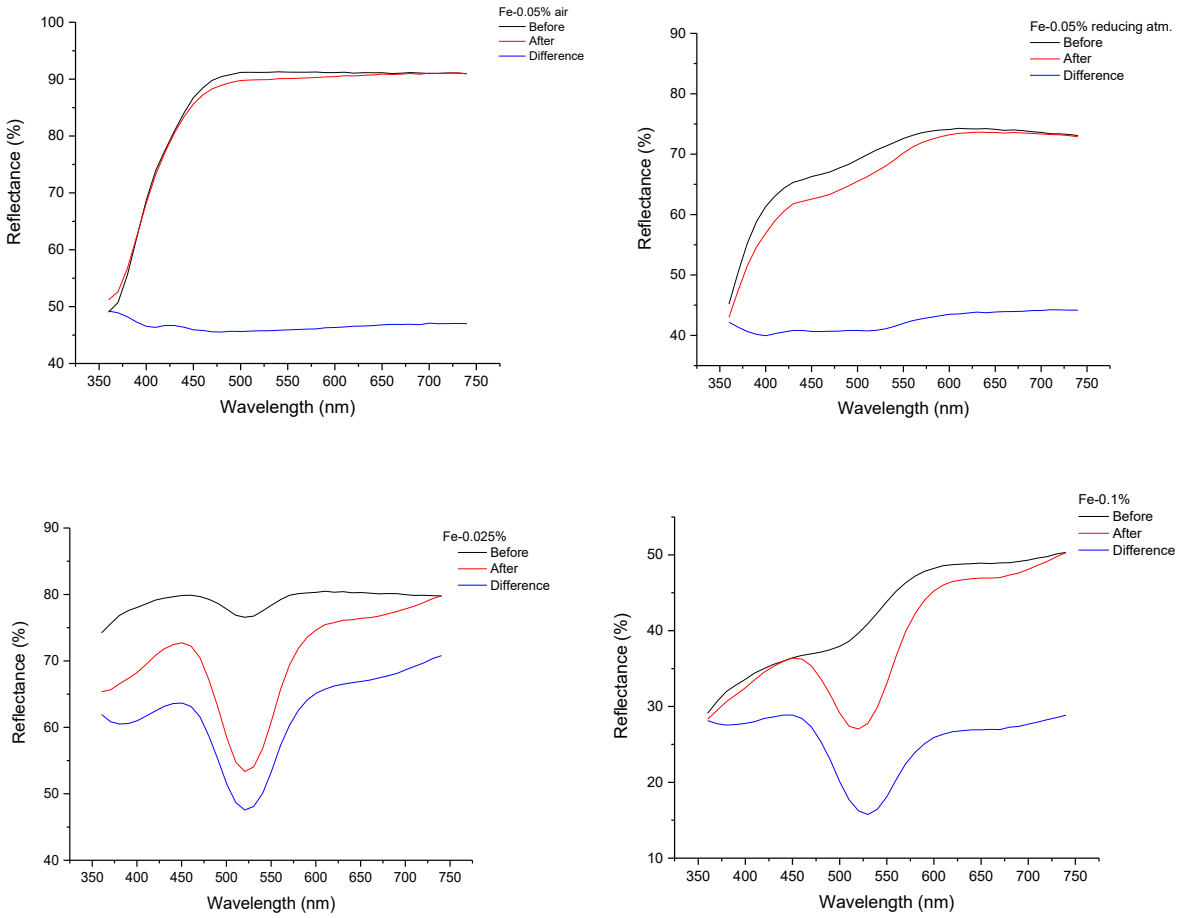

Figure 5. Reflectance spectrum of Fe-doped samples exposed to 254 nm UV light.

Figure 6 represents the photochromism on Fe-doped samples with different concentrations. It is visible that the most promising material in terms of photochromism among Fe-doped BMSs is a two-times-halved concentrated sample (0.025%).

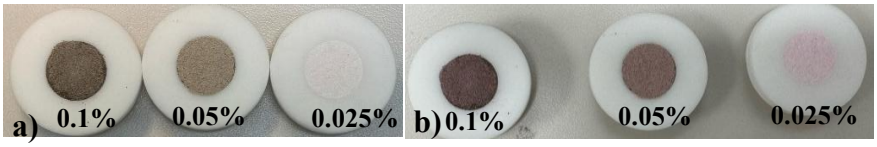

Figure 6. Fe-doped samples with different concentrations; a) before and b) after 5 min. 254 nm UV exposure.

We can also compare the reaction conditions for the Fe-doped sample with the same concentrations. Figure 7 shows the comparison of two samples of BMS:Fe-0.05% synthesized using different reaction conditions before and after exposure to 254 nm UV light.

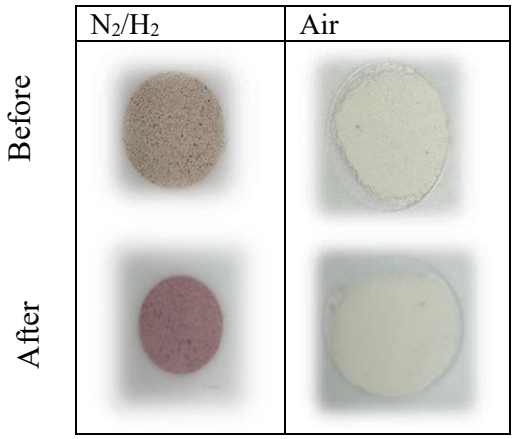

Figure 7. Comparison of the photochromism of two materials with the same composition but with different reaction conditions, with exposure to 254 nm UV light.

Samples exhibit intense differences in reflectance. Greater UV absorption suggests greater interaction with light, which can be useful in UV-based applications. All Co-doped samples show an adsorption peak around 475 nm within the blue region. The modification of absorption features also demonstrates that the variation of dopant concentration and atmospheric conditions modifies

the electronic structure and optical properties of the material and demonstrates their utility in tuning the material for a specific application (Fig. 8).

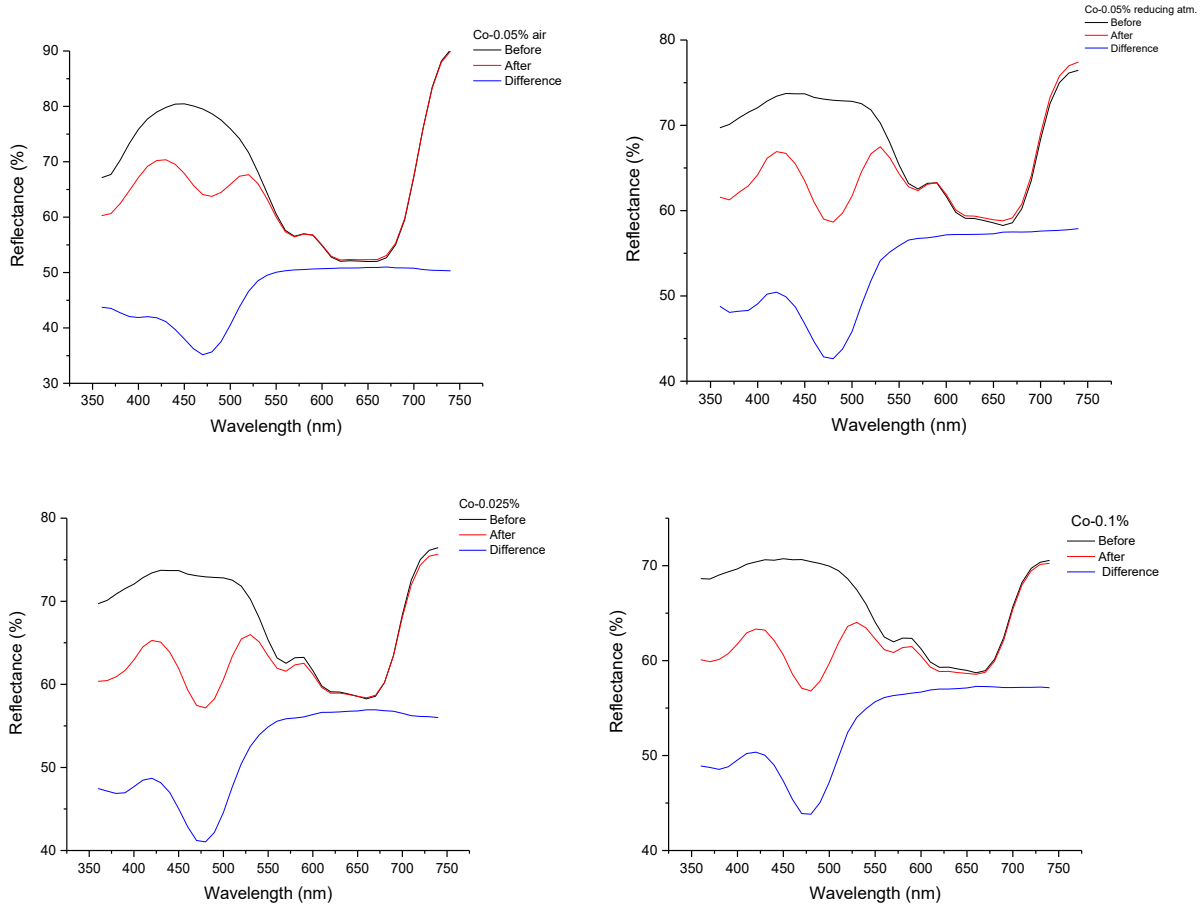

Figure 8. Reflectance spectrum of Co-doped samples exposed to 254 nm UV light.

Although the air-synthesized material is stable and has no significant color change, the reducing-atmosphere-synthesized samples have significant changes in their reflectance spectra. The larger this change, the more prominent it becomes at higher Cr contents, showing that the dopant concentration as well as atmospheric conditions are crucial factors for enhancing the optical behavior of the material.

Figure 9 shows the reflectance spectrum of the Cr-doped sample with different concentrations and the reaction atmospheres.

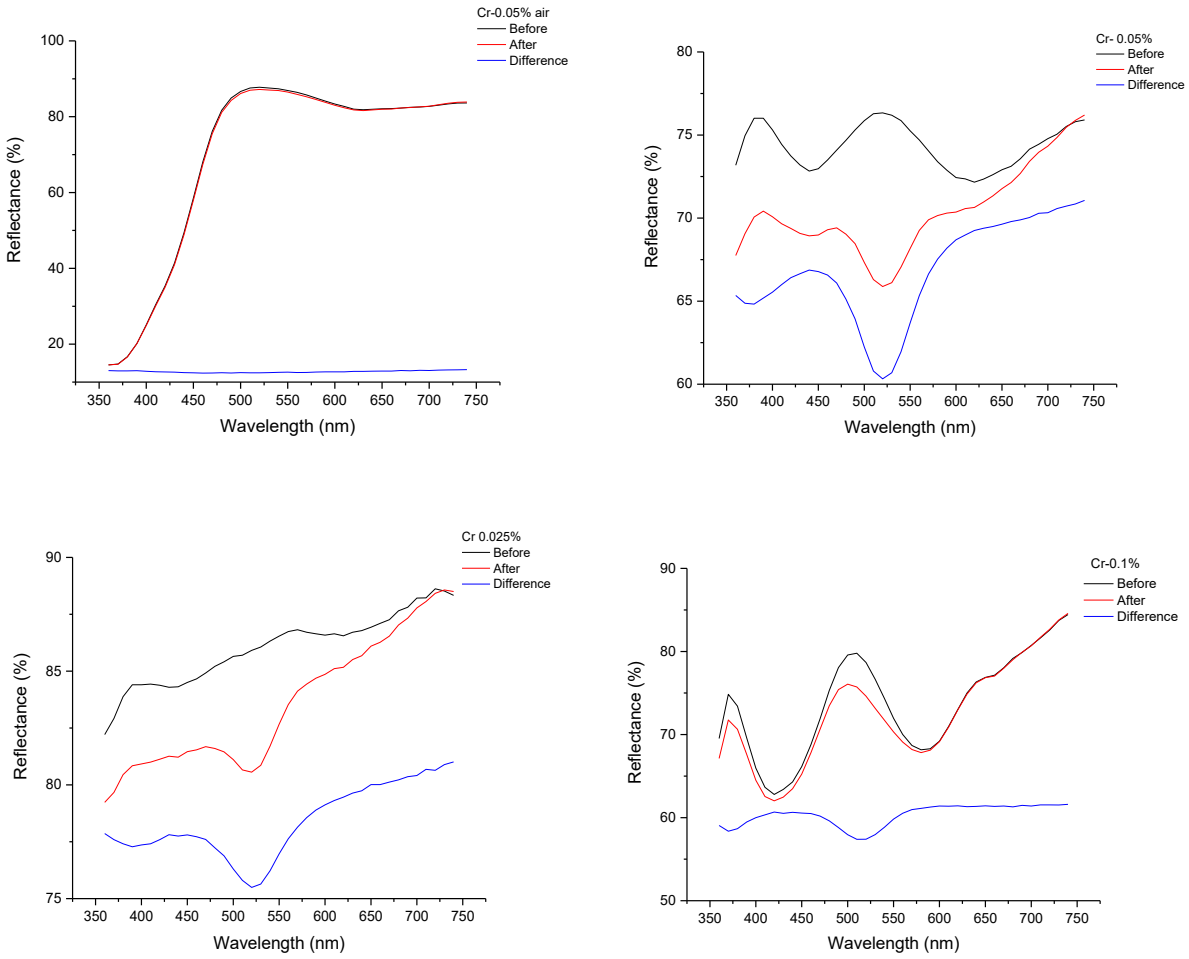

Figure 9. Reflectance spectrum of Cr-doped samples exposed to 254 nm UV light.

The Mn-doped samples have a slight absorption difference seen under 254 nm UV compared to 302 nm. The reaction condition and dopant concentration effects are most promising with shorter excitation wavelengths, where there is a steep reflectance change as a function of reducing environment and dopant variation (Fig.10).

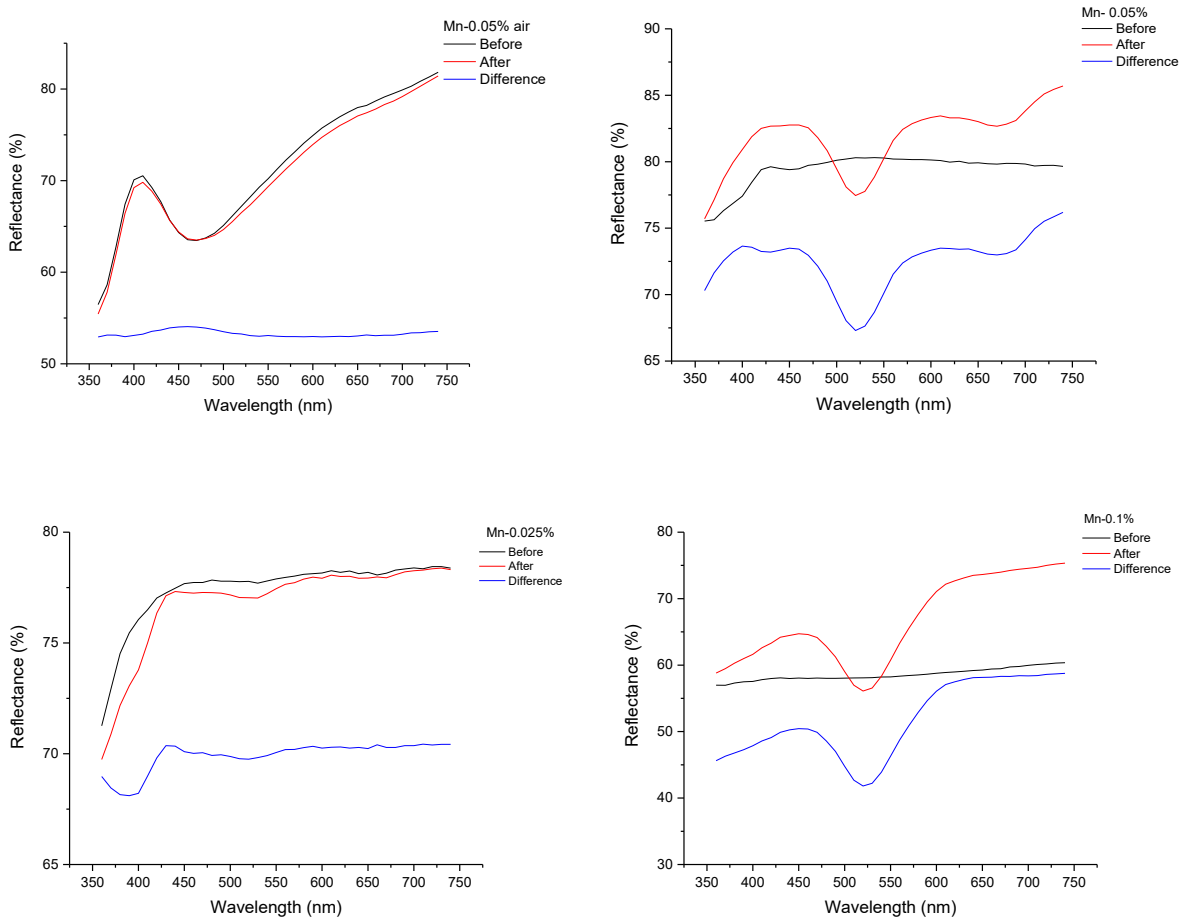

Figure 10. Reflectance spectrum of Mn-doped samples exposed to 254 nm UV light.

For Fe-doped samples, there is a slight absorption difference seen under 254 nm UV compared to that for 302 nm. The reaction condition and dopant concentration effects are most promising at 254 nm, where there is a steep reflectance change as a function of reducing environment and dopant variation around 525 nm within the green region. Again, the air-sintered sample is not as promising as the reducing atmosphere-sintered samples for Fe-doped material (Fig.11).

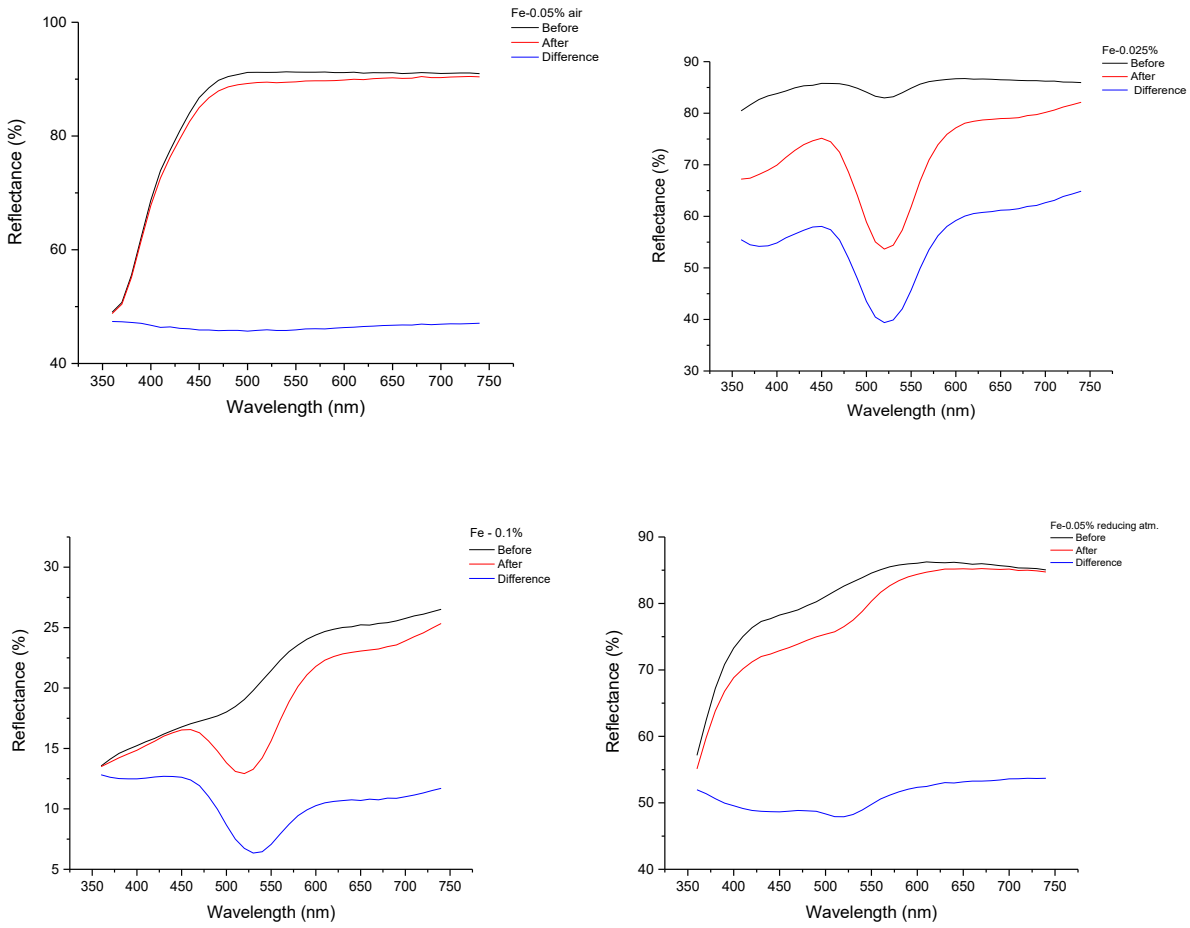

Figure 11. Reflectance spectrum of Fe-doped samples exposed to 302 nm UV light.

Figure 12 shows that the reflectance change in the Co-doped samples is greater under 254 nm UV exposure compared to 302 nm. Both dopant concentration changes and the reaction conditions significantly influence reflectance, with enhanced spectral shifts at 254 nm. At 302 nm, the difference is less apparent, which is indicative of reduced absorption and interaction. This indicates that the Co-doped materials are more sensitive to UV exposure at elevated energies.

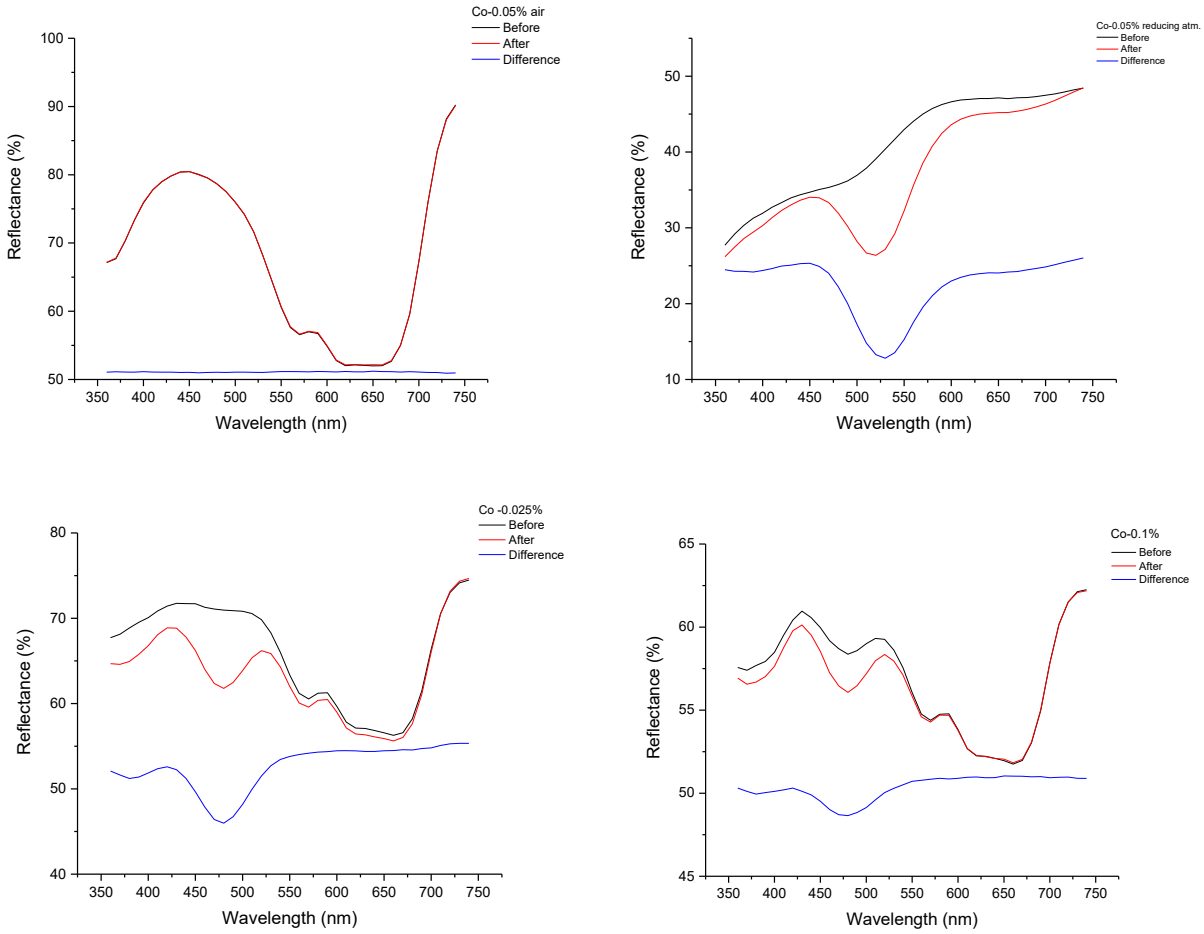

Figure 12. Reflectance spectrum of Co-doped samples exposed to 302 nm UV light.

The spectra of the Cr-doped samples show promising peaks with 254 nm UV light compared to 302 nm. Under 254 nm excitation, the effect of reducing atmosphere and dopant concentration is greater, generating more diverse differences in reflectance. The effects are less pronounced at 302 nm, with implications of decreased optical absorption and interaction. This is consistent with the observations of Fe- and Co-doped samples, where 302 nm UV light induces less extreme reflectance changes (Fig.13).

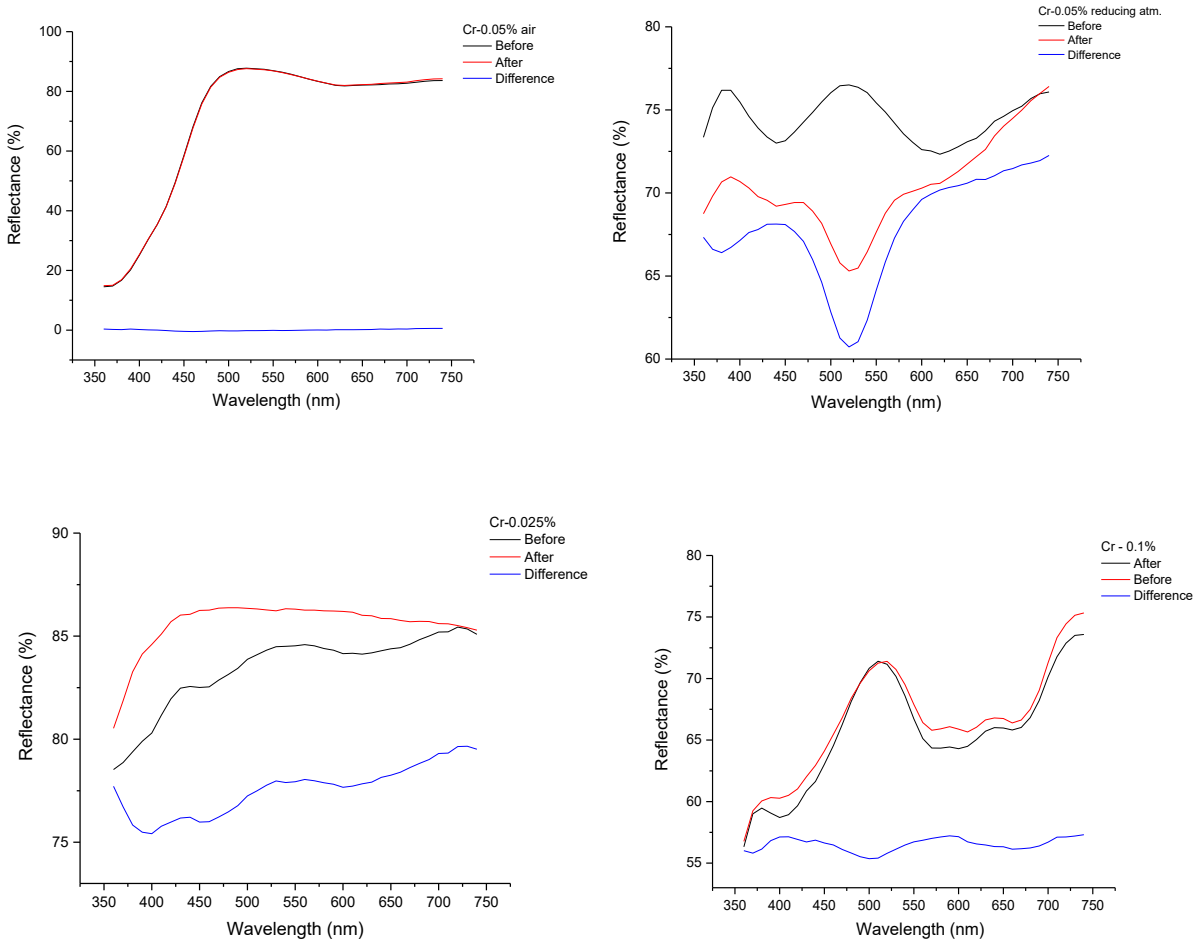

Figure 13. Reflectance spectrum of Cr-doped samples exposed to 302 nm UV light.

The reflectance spectra of the Mn-doped samples show a strong response to ultraviolet irradiation at 302 nm, compared to the more intense interaction at 254 nm. The influence of the reducing atmosphere in combination with the dopant amount is more intense at 254 nm, inducing strong reflectance variations. At 302 nm, the variations are not so extreme, showing a weaker absorption and interaction with light in comparison to the above-described samples (Fig.14).

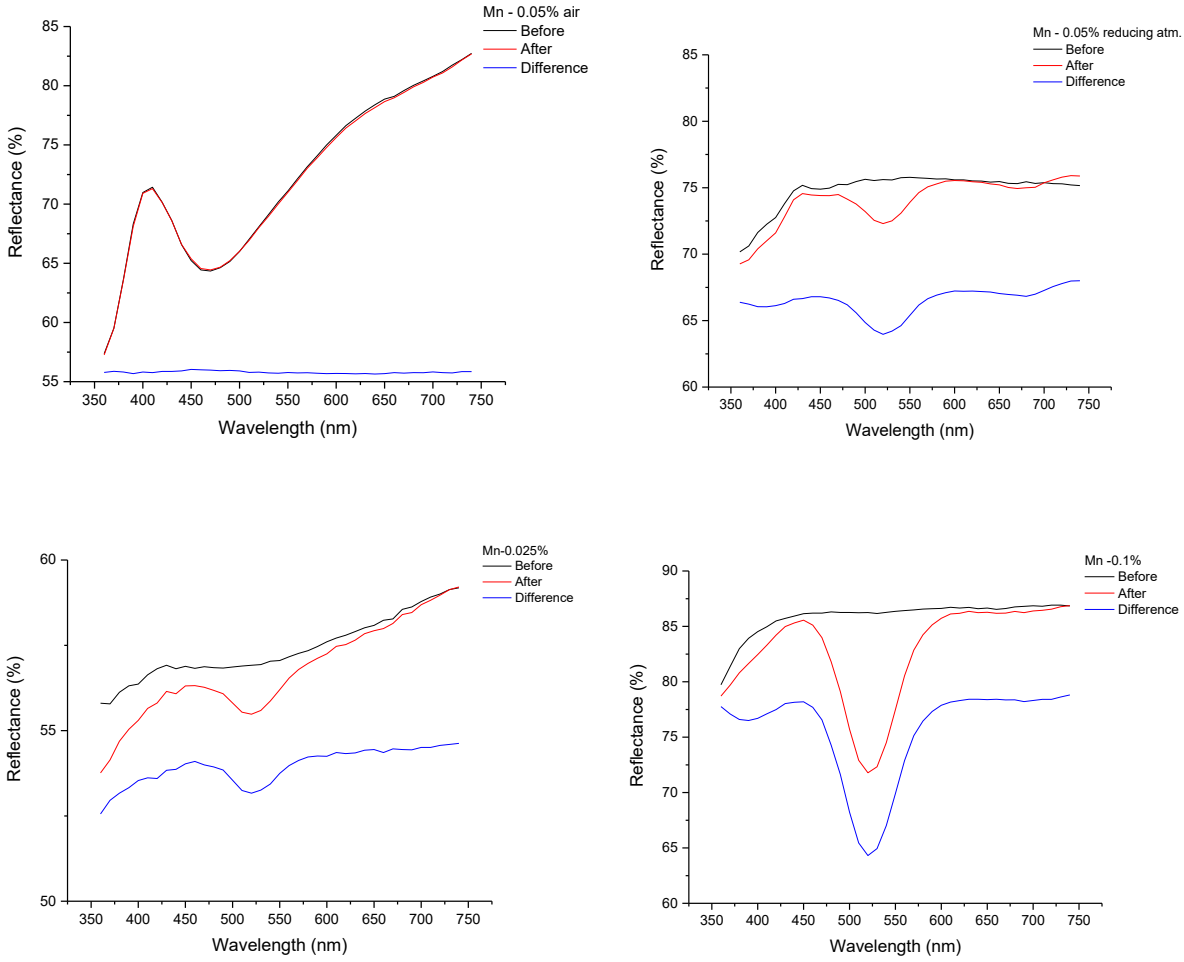

Figure 14. Reflectance spectrum of Mn-doped samples exposed to 302 nm UV light.

Figure 15 shows that the Fe-doped samples with 365 nm UV exposure are less colored than those with 302 and 254 nm due to energy-related colorations. So, in Figure 15, the most promising coloration happens in the samples with a reducing atmosphere. The reaction condition with air is not as successful as the reducing atmosphere due to the possible creation of oxygen vacancies. The most visible changes were primarily shown in samples with a 0.025% amount for all wavelengths. It was tested that Fe-0.025% is still the best option among all concentrations for this dopant.

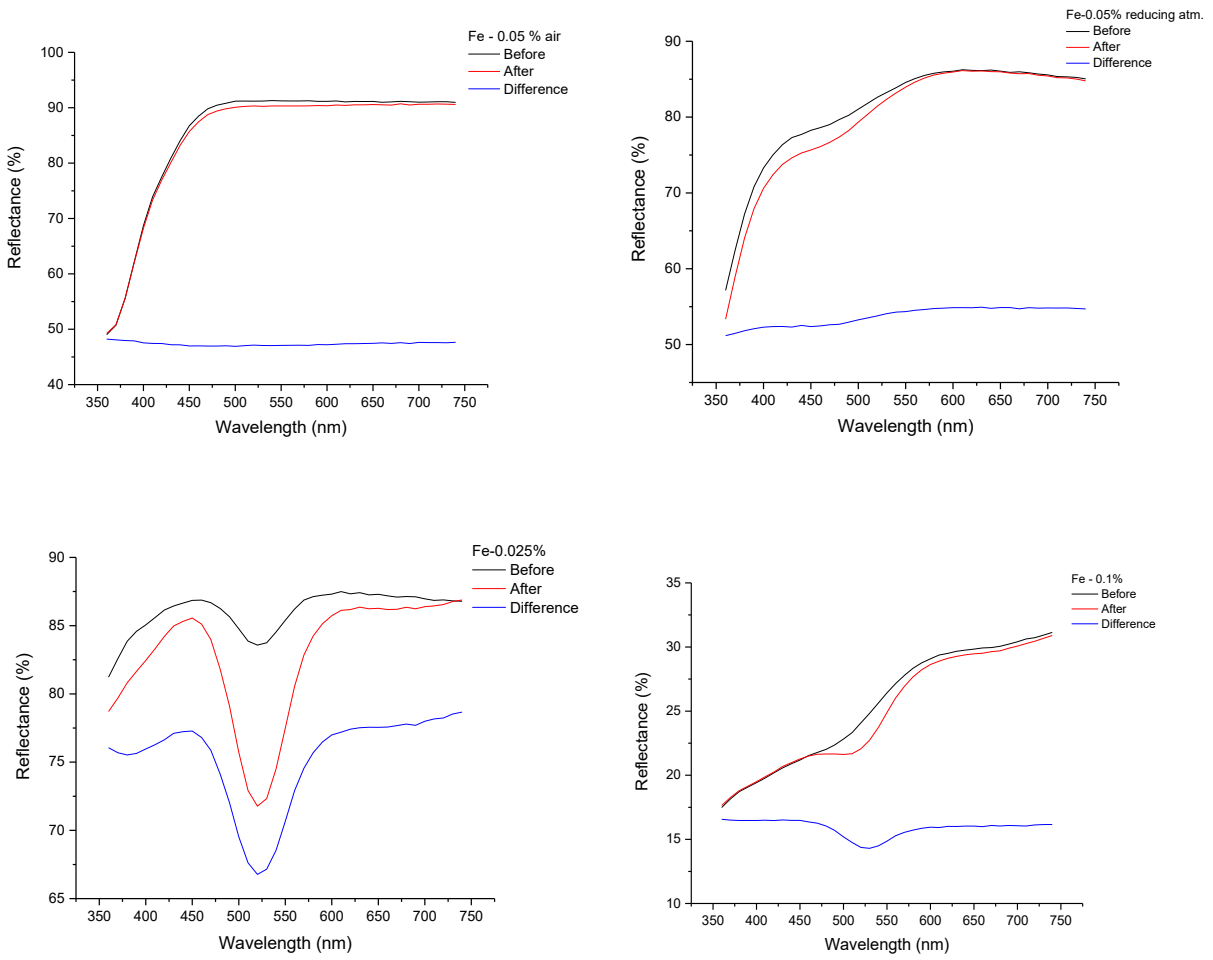

Figure 15. Reflectance spectrum of Fe-doped samples exposed to 365 nm UV light.

The Cr-doped samples irradiated with 365 nm mostly show no color change at all, while there is only a slight change in the Cr-0.05% sample, which is quite similar to the Fe and Mn cases. Unlike Fe-doped samples, 0.025% Cr does not exhibit spectral changes. This shows that the interaction between dopant and UV exposure is more dependent on dopant concentration and atmospheric conditions (Fig.16).

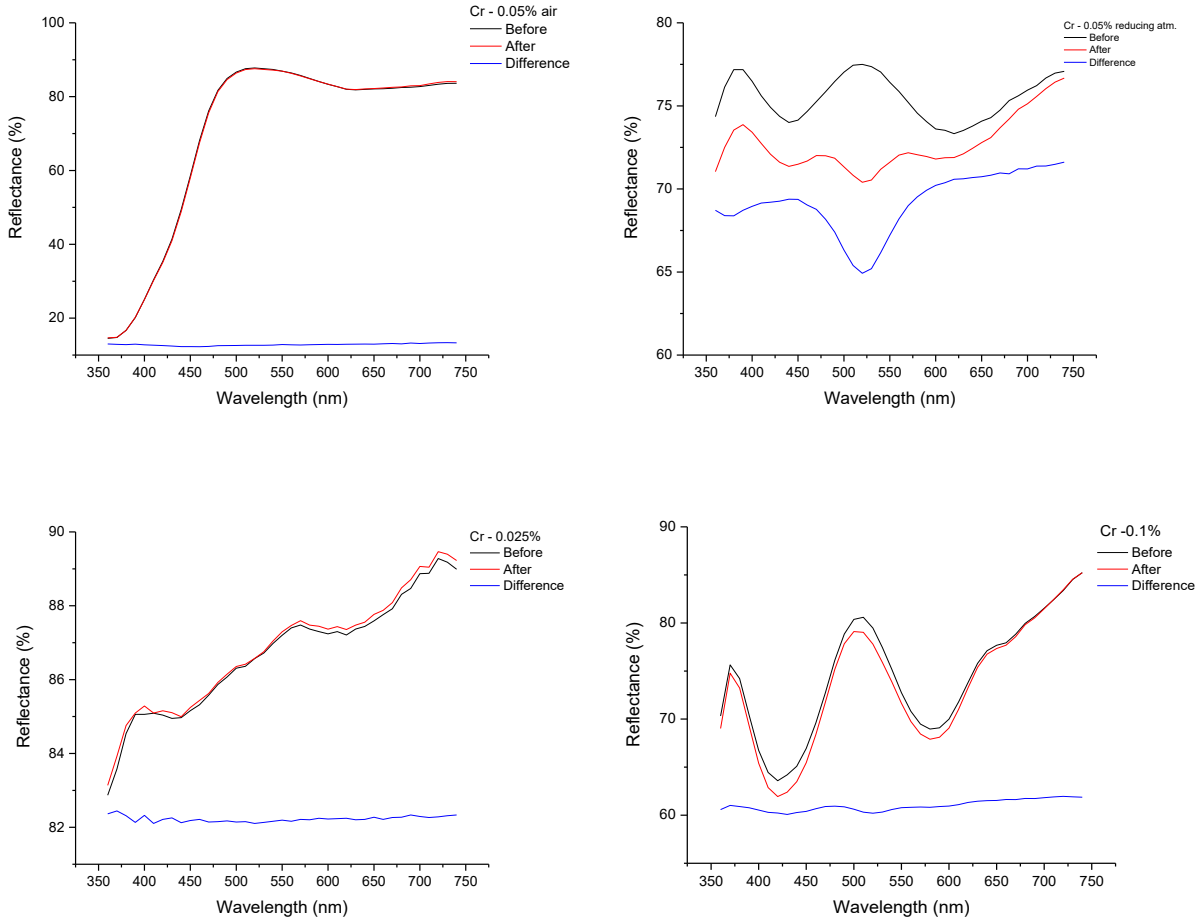

Figure 16. Reflectance spectrum of Cr-doped samples exposed to 365 nm UV light.

Figure 17 shows that Co-doped samples have different properties from others; most of the adsorption peaks appear around 475- 525 nm. Furthermore, 0.025% dopant concentration is similar to Fe, which shows the most significant changes, while 0.1% has minimal impact among those samples. The reducing atmosphere on this occasion still shows better performance than the air-synthesized sample.

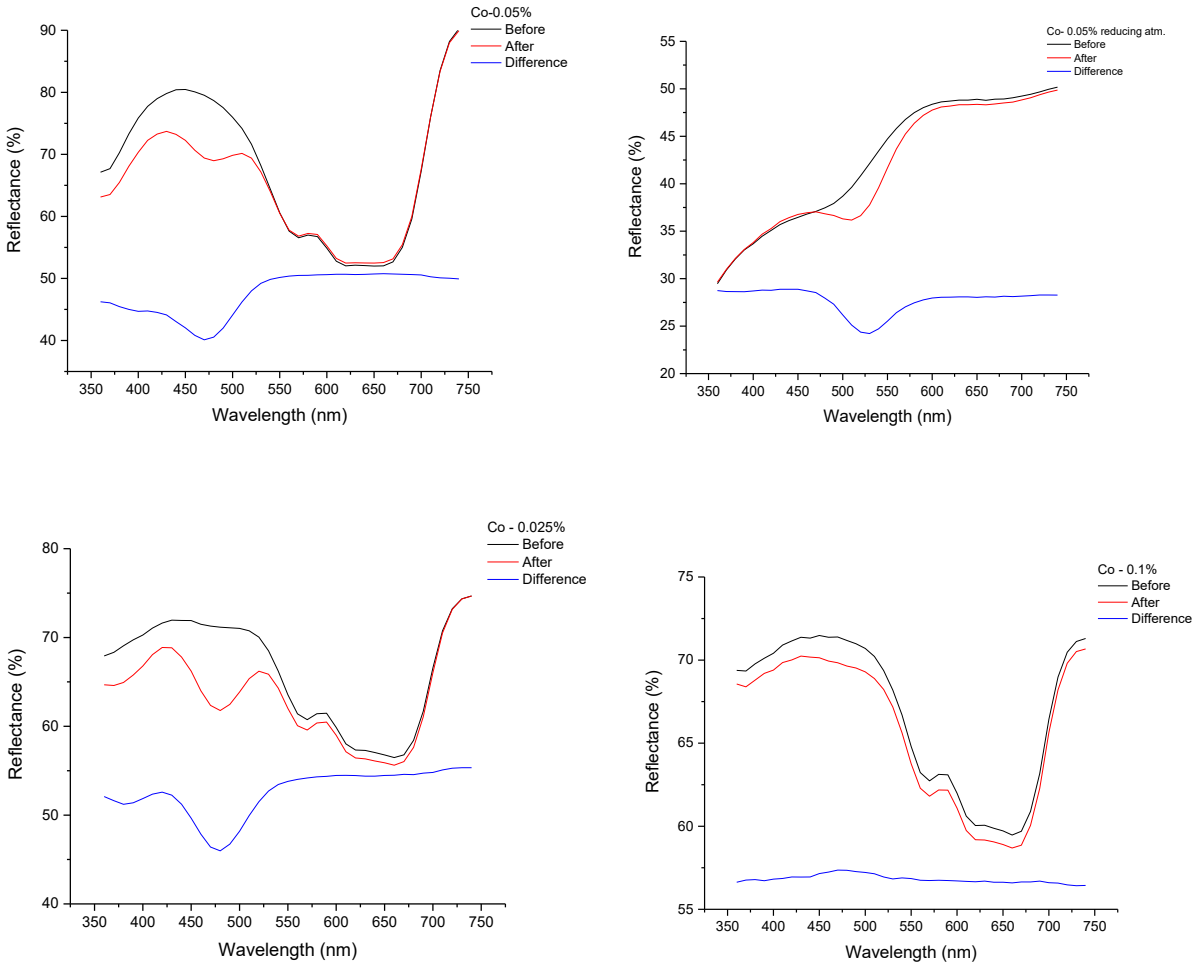

Figure 17. Reflectance spectrum of Co-doped samples exposed to 365 nm UV light.

In Figure 18, it is visible that the spectra of Mn-doped samples show that doping concentrations and reaction conditions highly affect the optical behavior of the samples. The air-synthesized 0.05% Mn-doped sample shows weaker coloration properties, while the material with 0.025% dopant concentration shows a little better response to 365 nm UV light.

Overall, UV-A light does not affect the coloration directly, as is shown in those graphs for doped samples with different concentrations.

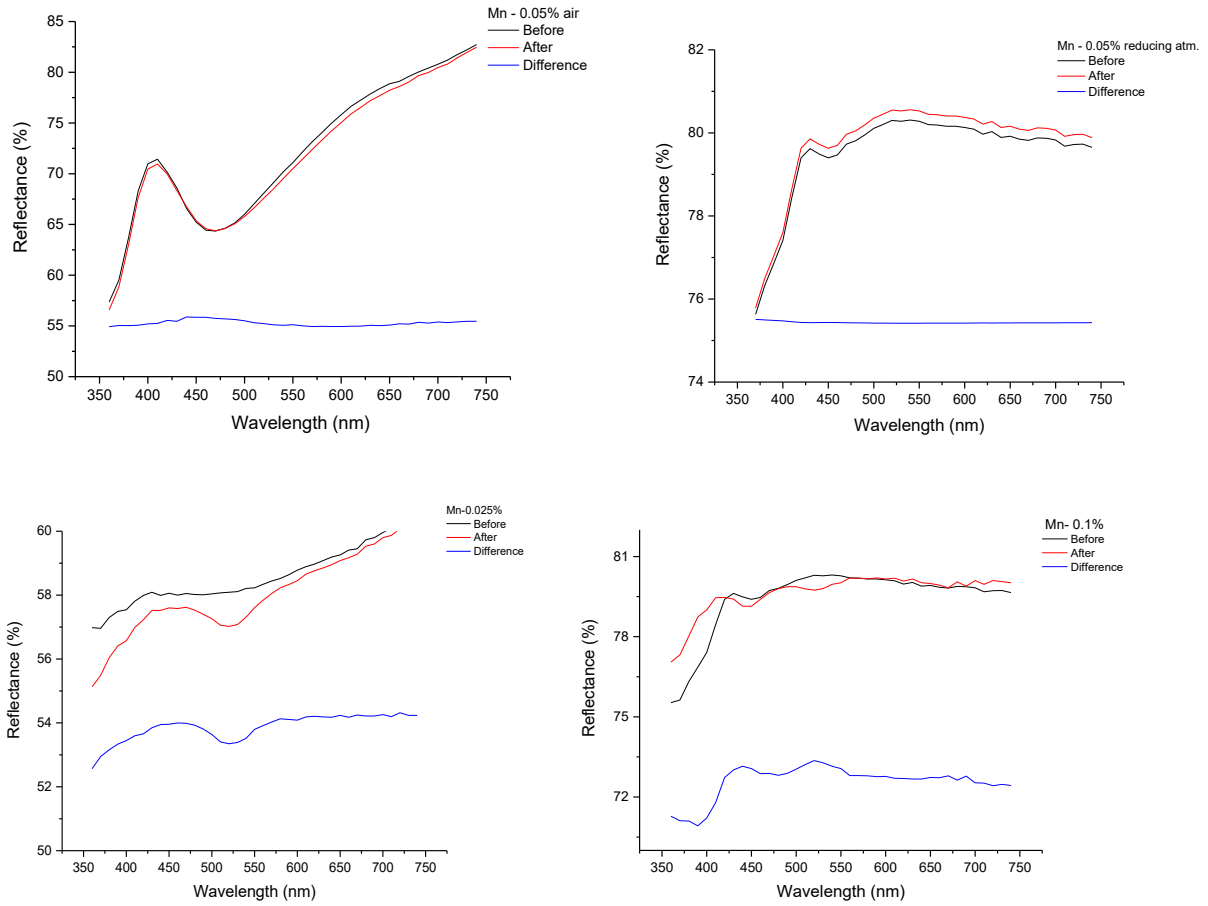

Figure 18: Reflectance spectrum of Mn-doped samples exposed to 365 nm UV light.

3.1.4. Luminescence Spectroscopy

After determining which reaction condition is the best for photochromism enhancement, further analyses were carried out with samples synthesized in a reducing atmosphere. The Varian Cary Eclipse spectrometer was used for luminescence measurements. The mode was phosphorescence, and the emission and excitation spectra of each sample with high and medium voltages were recorded. The complete phosphorescence decay was 0.0051 seconds. During emission spectrum measurements, excitation wavelengths were set at 254, 302, and 365 nm to test the highest emission peak.

Figure 19 depicts excitation and emission spectra of Co-doped samples of varied concentrations (0.025%, 0.05%, and 0.1%) with the pictures of the samples. The sharp emission peaks at 500–520 nm on excitation at 302 nm are anticipated to result from d-d transitions of Co^{2+} ions in the host matrix. The excitation spectra of the matching bands are wide UV bands characteristic of Co^{2+}-related transitions. As dopant concentration increases, emission intensity changes, and slight spectral variations are observed.

Several emission wavelengths (700 nm, 600 nm, and 435 nm) are also visible at 0.05% Co, and this is probably a possible contribution from different luminescence centers. Furthermore, doping with Co affects the optical behavior of the material, with the most intense and precise emission seen at lower concentrations (most significantly 0.025%).

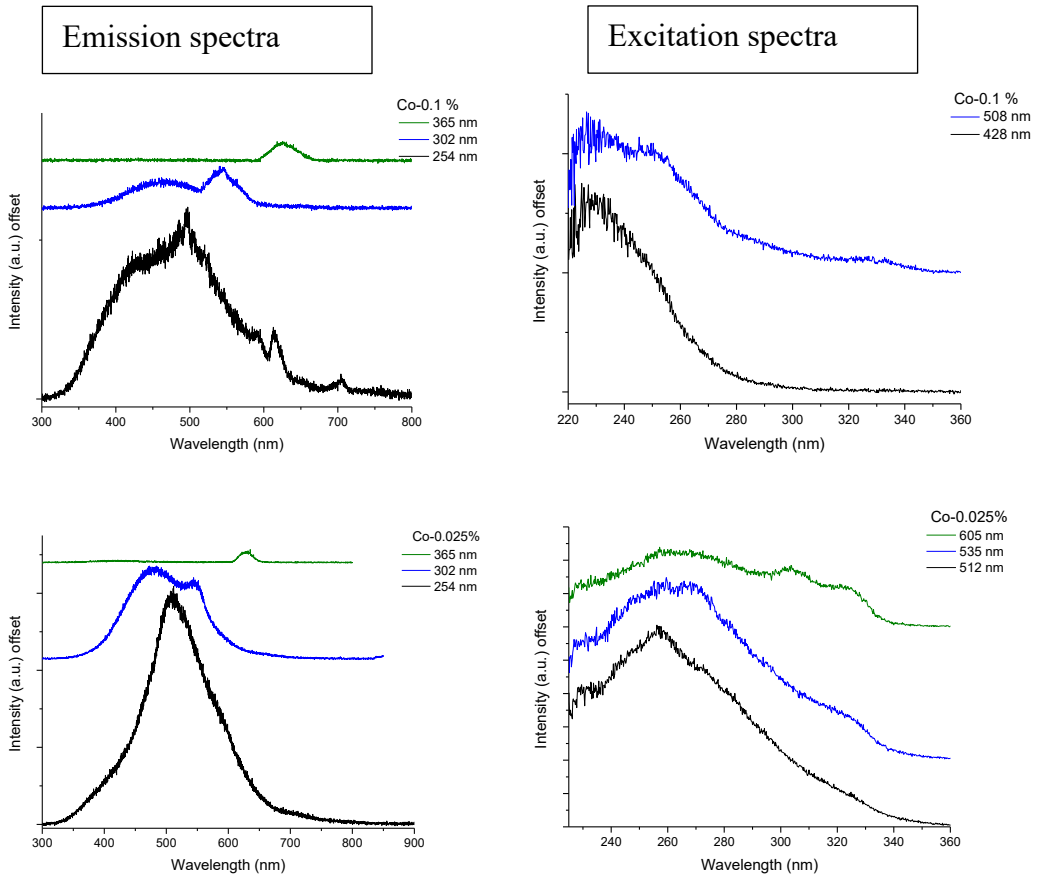

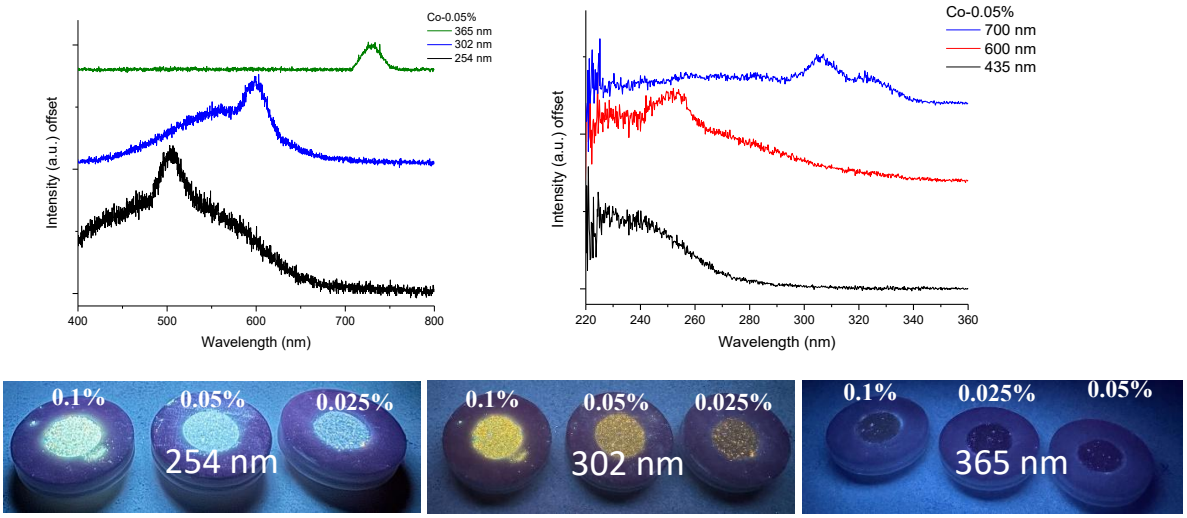

Figure 19. Excitation and Emission spectra of Cr-doped samples with different dopant concentrations and photos with three different excitation wavelengths (254, 302, and 365 nm).

When we look at Figure 20, it is observable that with increasing dopant concentration up to 0.05%, further emission peaks are observed at longer wavelengths (600 nm and 725 nm), which might be the formation of new luminescent sites or altered Cr^{3+} surroundings. Decreasing emission intensity is observed with Cr-0.1%, where concentration quenching phenomena lead to energy transfer between closely situated Cr^{3+} ions to cause non-radiative decay.

The most intense and well-defined emissions occur at lower concentrations (particularly 0.05%). It shows the important role of dopant concentration in controlling luminescent behavior.

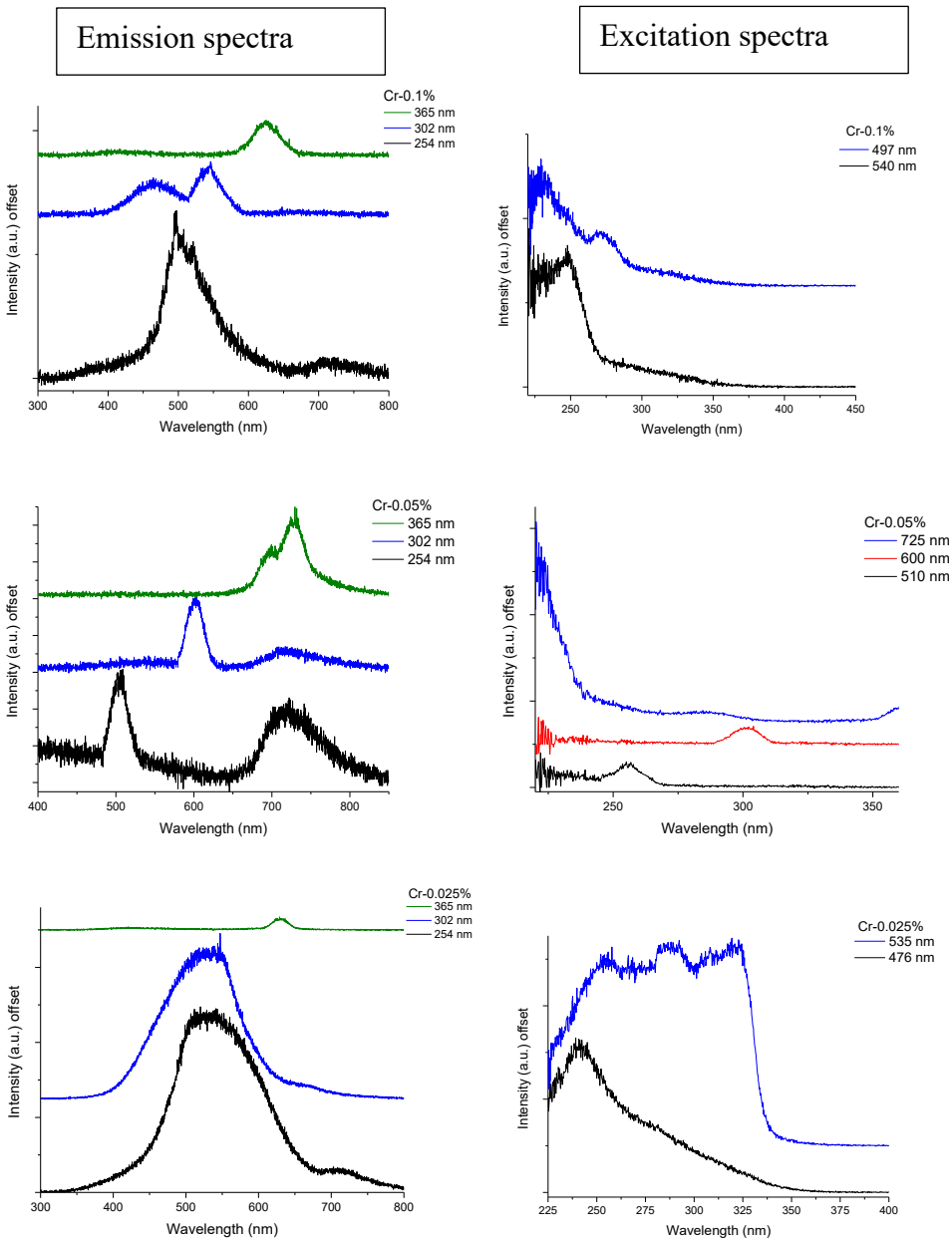

Figure 20. Excitation and Emission spectra of Cr-doped samples with different dopant concentrations

The shifts and excitation peaks show that the Fe ion alters the optical properties of the material. The appearance of longer-wavelength emissions at higher concentrations points to possible interactions between neighboring Fe ions or changes in local crystal field symmetry. These results show the role of dopant concentration in controlling the emission color and efficiency. Again, the most prominent peak can be seen around 500-510 nm wavelengths, which probably comes from the dopant for all samples. The most distinct behavior can be seen in the Fe-0.025% sample with

four different emission wavelengths (493, 506, 600, and 700 nm), while Fe-0.1% only has one peak that comes from the monochromator at around 500 nm (Fig.21).

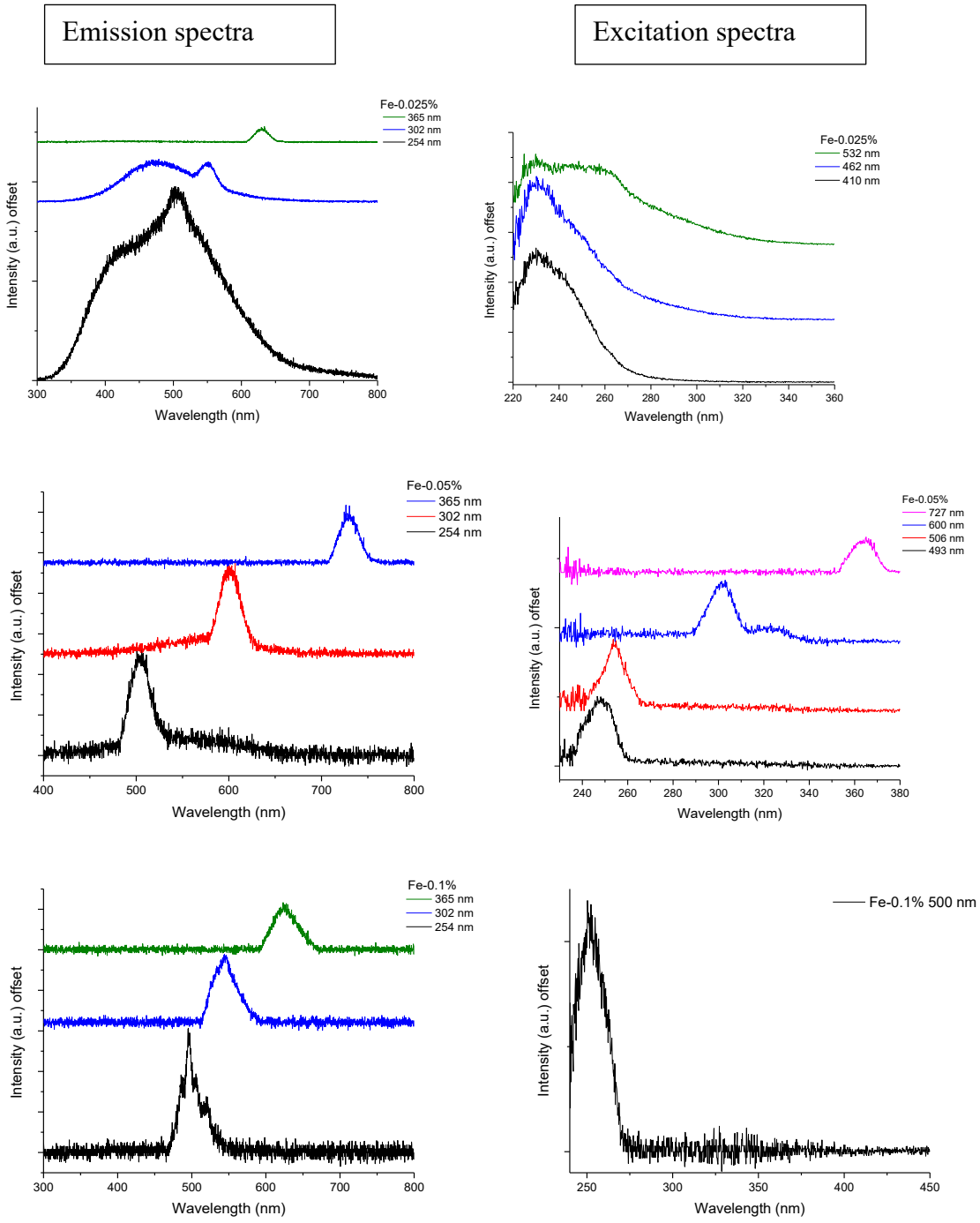

Figure 21. Excitation and Emission spectra of Fe-doped samples with different dopant concentrations.

The difference between excitation and emission spectra implies that concentration and dopant choice affect the optical characteristics. Emission peaks at 0.1% concentrations can be an indicator of the transfer of energy between ions, which affects luminescent characteristics. The most prominent peak is visible at the Mn-0.1% sample, which is excited by 254 nm UV light around the 552 nm region. The most distinct behavior can be seen in the Mn-0.025% sample with three different peaks around 402-530nm (Fig.22).

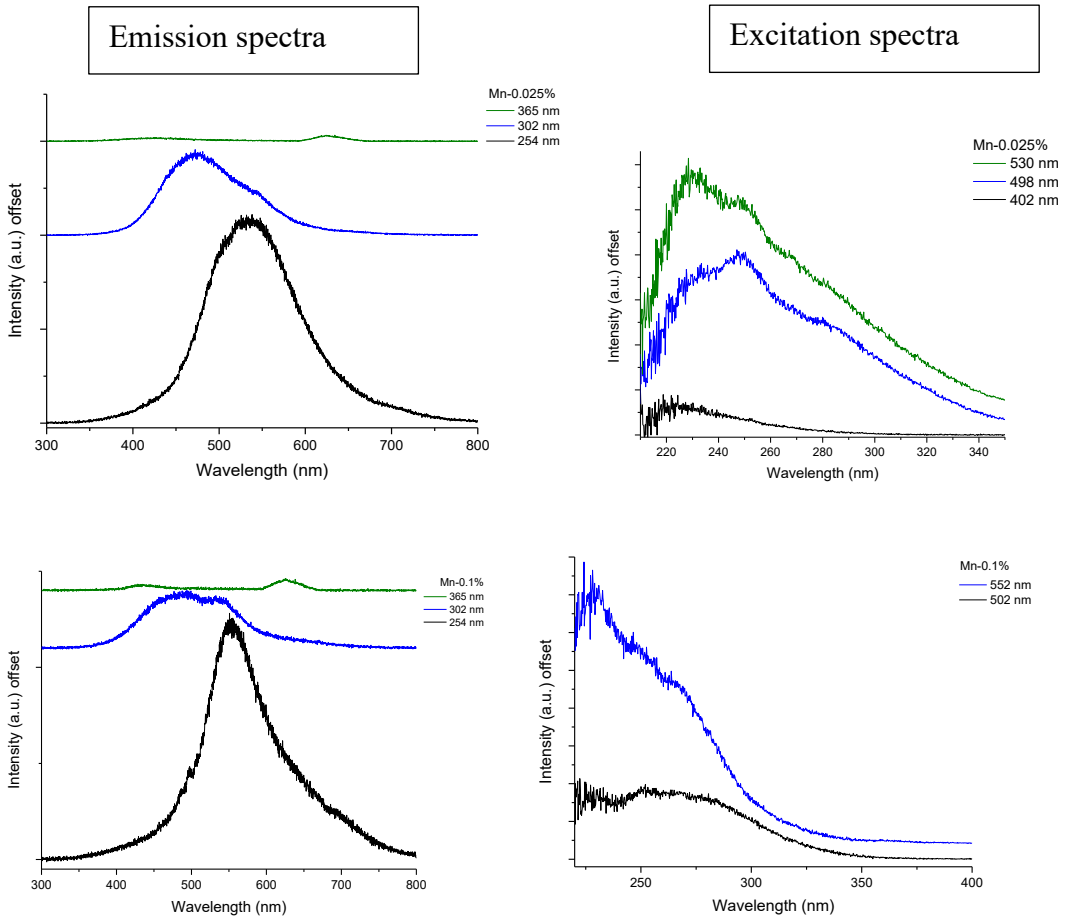

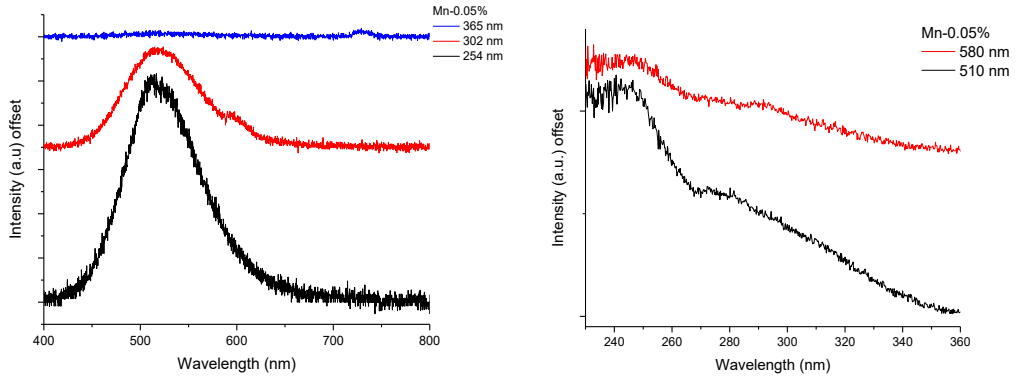

Figure 22. Excitation and Emission spectra of Mn-doped samples with different dopant concentrations.

Persistent luminescence (PeL), in other words, "afterglow" measurement was done with an Eu-doped sample, which has strong light after removing the excitation source. A one-minute waiting time between each measurement followed. The measurement in bio-/chemiluminescence mode, using a 20 nm emission slit, 1.0 nm data interval, and high PMT voltage. Figure 23 shows that the Eu-doped sample exhibits PeL with three different wavelengths (254, 302, and 365 nm).

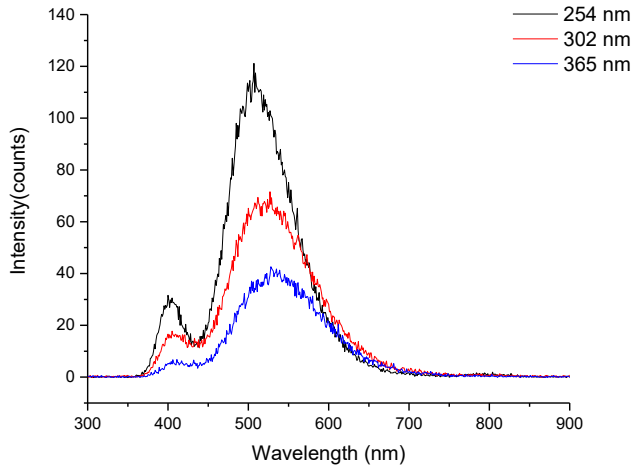

Figure 23. PeL spectrum for Eu-0.05 % sample.

3.1.5. X-Ray dosimetry analyses

X-ray and UV-exposure analyses were conducted to find out the applicability of the material for dosimetry-related applications. Various concentrations of doped BMS were tested, showing that the material is applicable for dosimetry analyses. However, the behaviors of dopants lead to variations in the results. These differences point to the influence of dopant type and concentration on the material's responsive properties. Each sample also demonstrates bleaching upon exposure to visible light for seven days, making it useful for different applications.

Different concentrations for X-ray exposure analyses were tested for the Fe-doped sample. As shown in Figure 24, as time passes, adsorption curves get deeper, which indicates the coloration processes for each graph. Fe-0.025% shows the most promising spectral changes, while the 0.1% sample has subtle variations. The bleaching curves show that the process is reversible, which confirms photochromism.

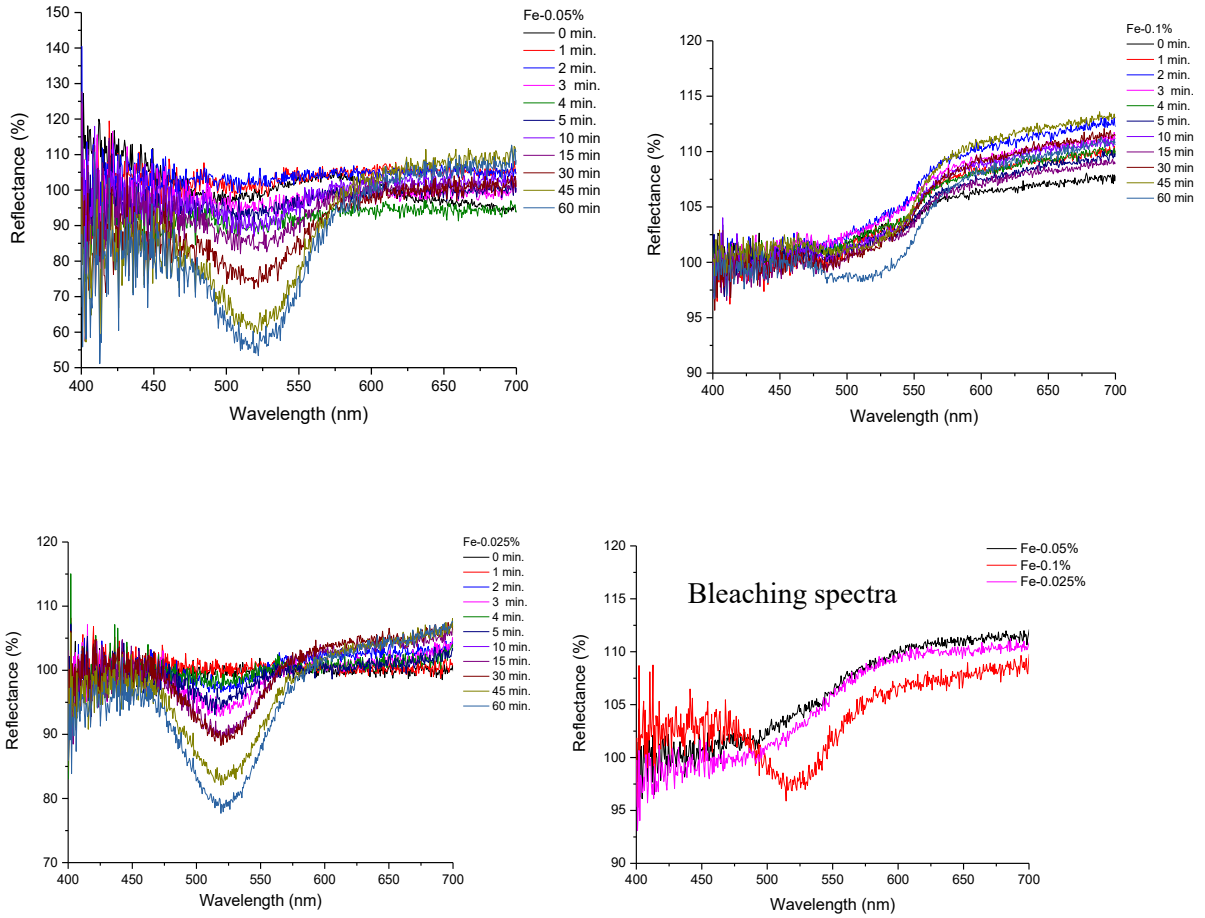

Figure 24. Reflectance curves of X-ray exposed Fe-doped samples with different dopant concentrations, coloration, and bleaching spectrum, respectively.

The Co-doped samples appear similar, but the sample at the concentration of 0.05% is slightly different. All the samples were colored when they were exposed to X-rays and bleached to their original color when they were under visible light for seven days.

This diverse behavior is responsible for Co ions having a different response in the lattice when irradiation is involved. This might be due to stable changes in their oxidation state or a predisposition to the formation of metallic clusters in high concentrations. These changes at lower concentrations indicate that single Co sites could be more effective in the formation of radiation-induced defects or being able to trap charges (Fig.25).

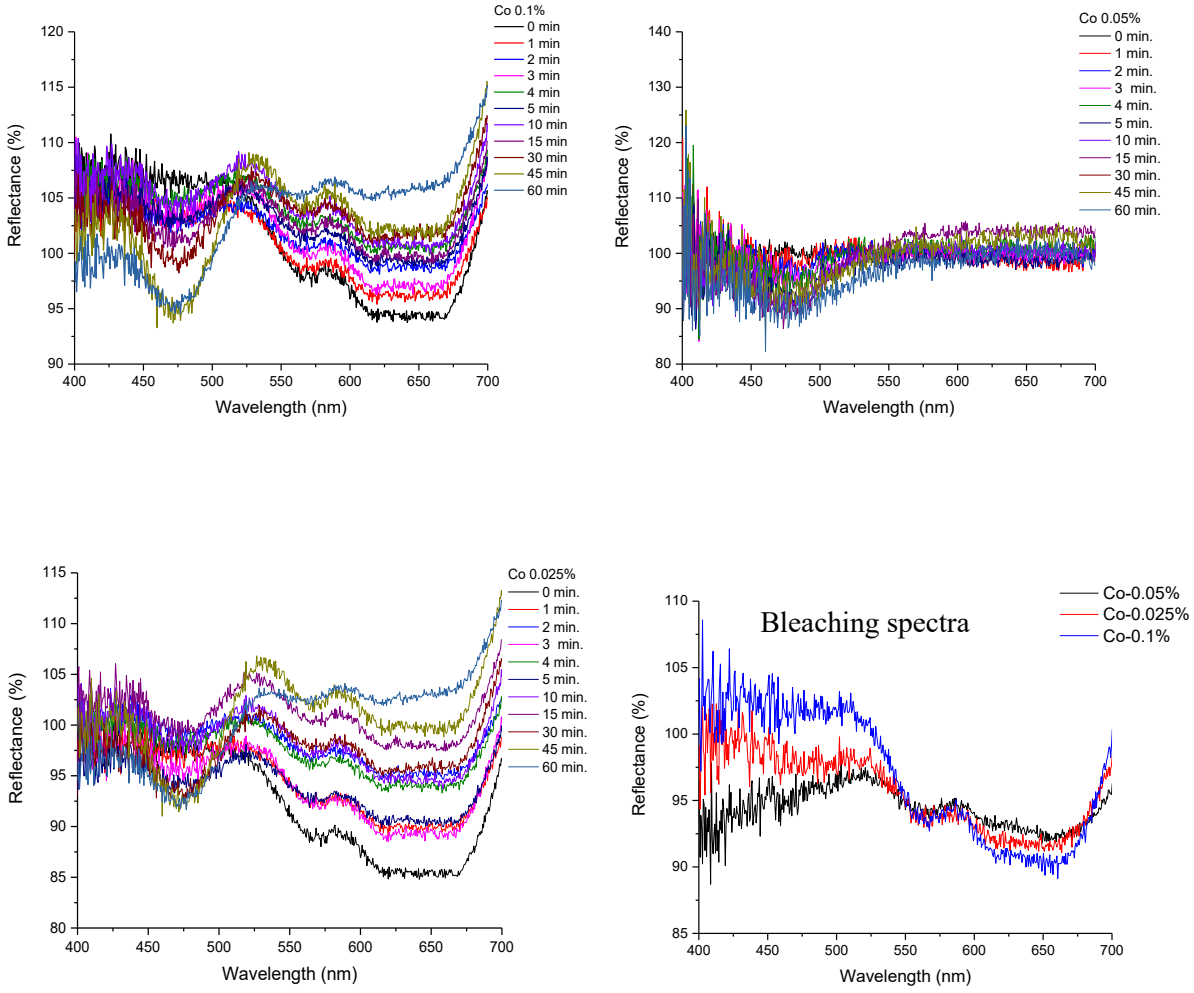

Figure 25. Reflectance curves of X-ray exposed Co-doped samples with different dopant

concentrations and bleaching spectrum.

Figure 26 shows that the reflectance curves of Mn-doped samples have some variations depending on the dopant concentration. The sample with a 0.1%-Mn doping level shows the most dramatic spectral changes, which might be an optimal concentration range because Mn ions actively participate in defect formation and charge transfer processes under irradiation. In contrast, both 0.025% and 0.05% doping concentrations have lower responses.

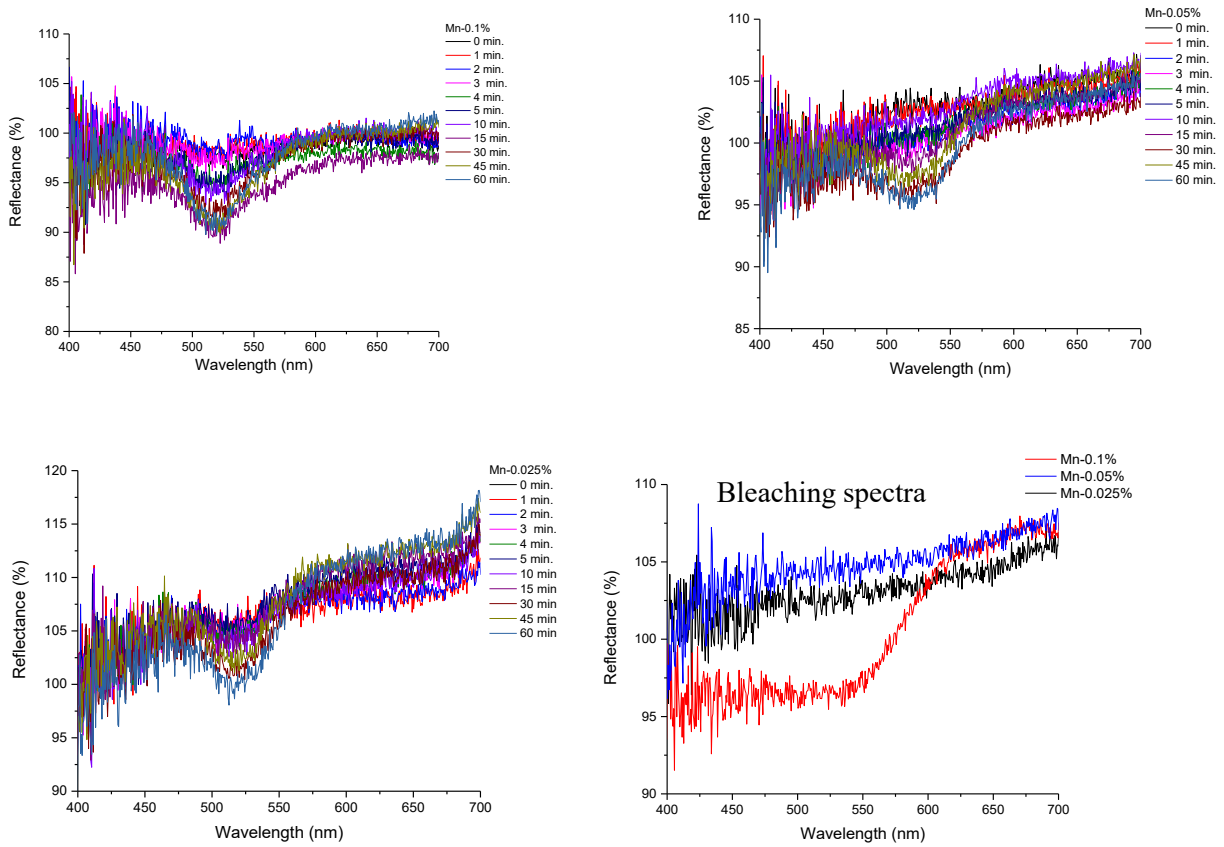

Figure 26. Reflectance curves of X-ray exposed Mn-doped samples with different dopant concentrations and bleaching spectrum.

The Cr-doped samples show some changes in their coloration and bleaching behavior when exposed to X-rays. Higher Cr concentrations (like 0.1%) have more visible shifts in reflectance over time. Moreover, Cr-0.025% does not exhibit strong coloration like others. Bleaching spectra are an indicator of reversible photochromism for Cr-doped samples (Fig.27).

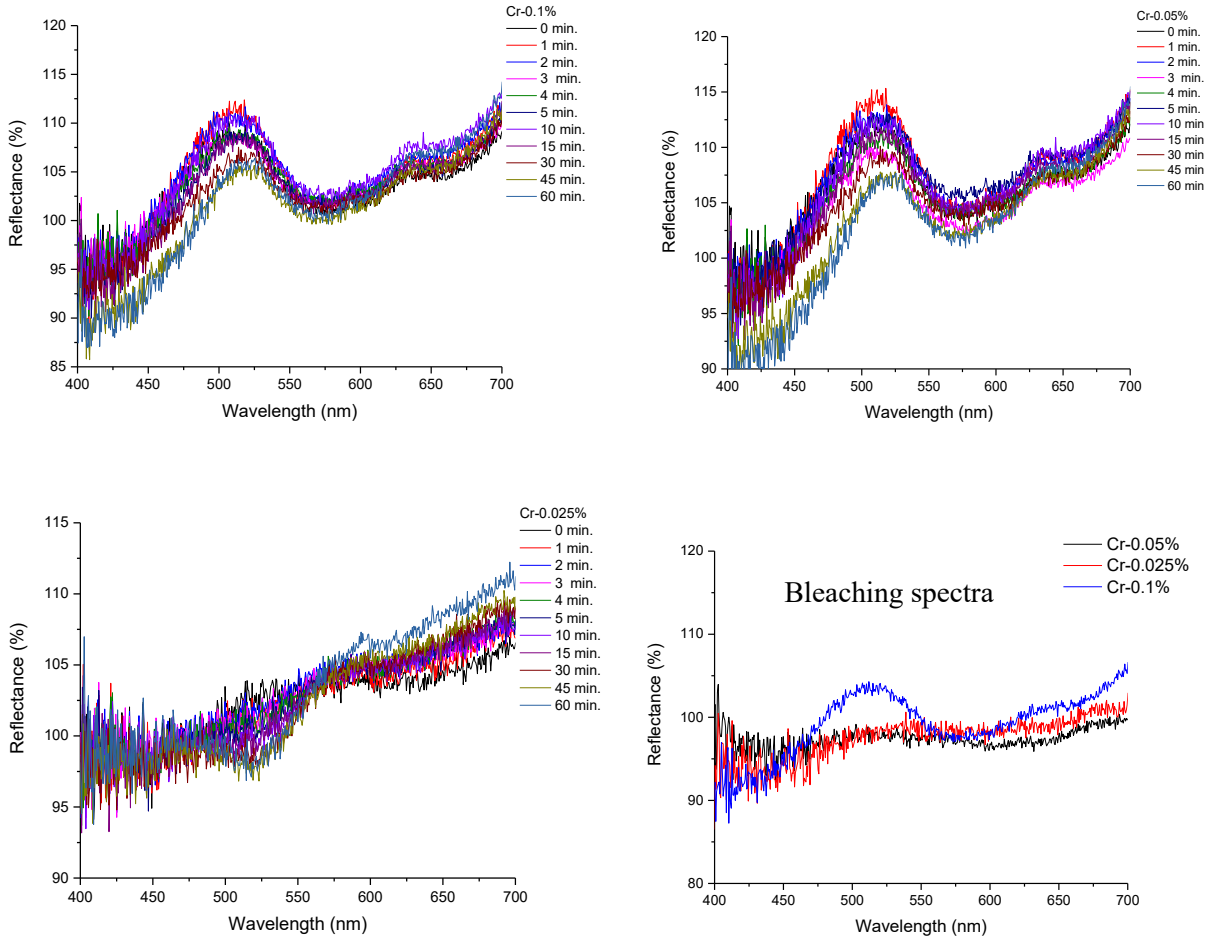

Figure 27. Reflectance curves of X-ray exposed Cr-doped samples with different dopant concentrations and bleaching spectra.

Overall, all samples are highly responsive to X-ray radiation and can be used in different X-ray dose quantification-related applications. The most promising and readable results come from Fe-doped 0.025% and 0.05% samples in terms of dose detection when we look at the curves (Fig. 24).

3.1.6. UV-exposure analyses

UV-exposure analyses were conducted to evaluate the potential of BMS for UV-related applications. To ensure thorough assessment, three distinct (254, 302, and 365nm) wavelengths of UV light were tested. These tests provided important insights into the interaction between doped BMS and UV radiation, especially for its color adsorption characteristics. The findings from these analyses help to a deeper understanding of the material's suitability for useful applications where UV exposure is a part of the study. This test was carried out for four different dopants (Fe, Mn, Cr, Co) with three different concentrations (mass-0.025%, 0.05%, and 0.1%).

3.1.6.1. Analysis with 254 nm

All three Fe-doped samples show a visible coloration change with increasing UV dosage. Among the samples, the "Fe-0.025 %" sample possesses the largest dynamic range. The observed responses are well suited to the desired characteristics of dosimetric materials: initial sensitivity, saturation response, and reproducibility (Fig.28).

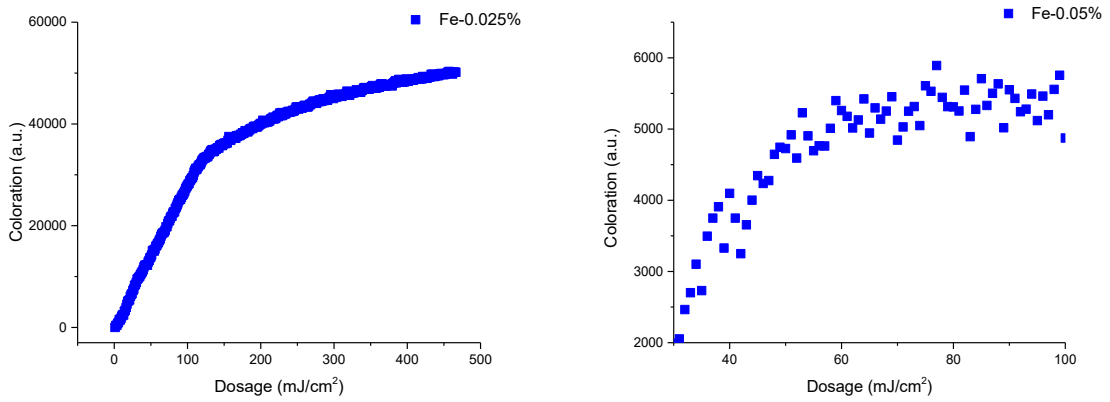

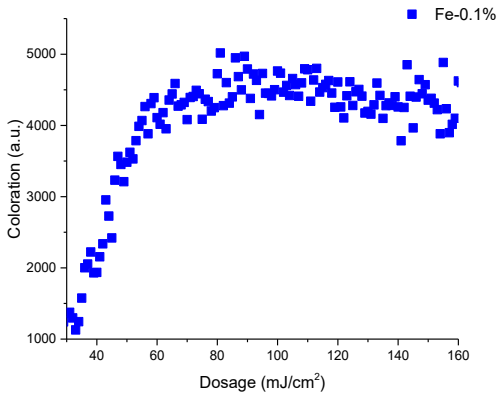

Figure 28. Dose quantification analysis of Fe-doped samples with 254 nm UV light.

The Co-doped materials also demonstrate strong potential for dosimetry applications under 254 nm irradiation. As shown in the plots, all three samples—Co-0.1%, Co-0.05%, and Co-0.025%—exhibit a clear and saturating coloration response. The Co-0.1% sample shows a wide dynamic range and gradual saturation up to 800 mJ/cm^2 (Fig.29).

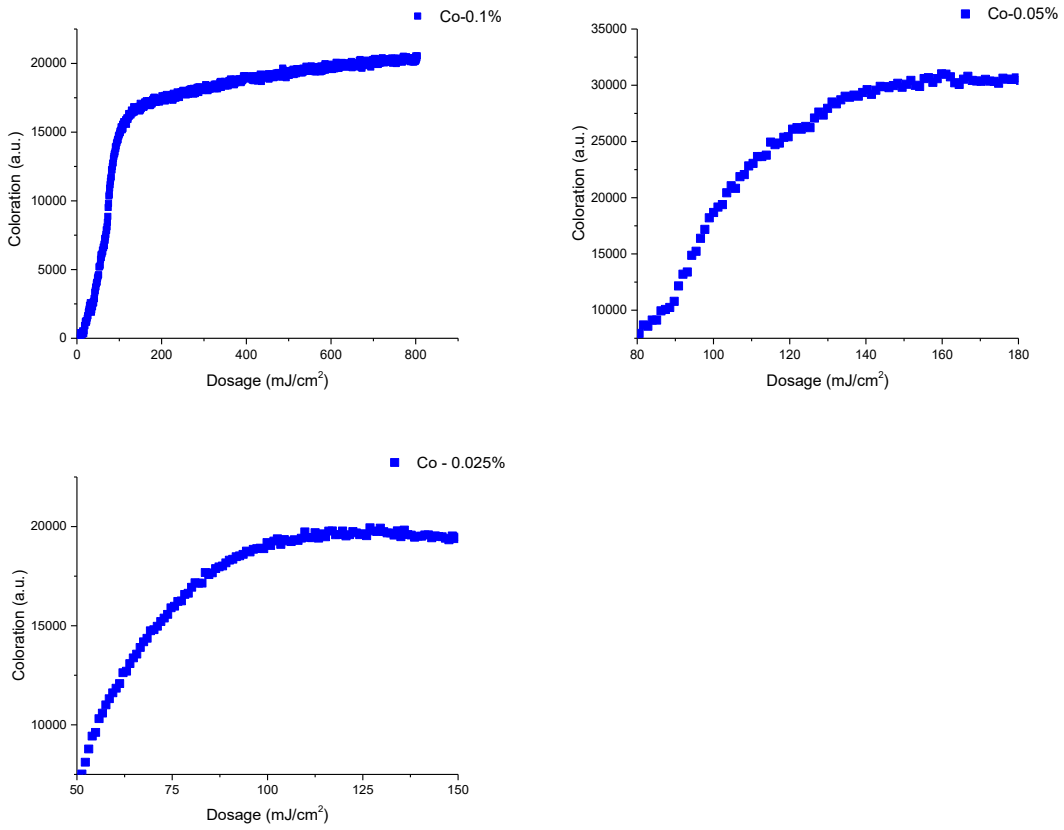

Figure 29. Dose quantification analysis of Co-doped samples with 254 nm UV light

Figure 30 shows that the Cr-doped materials show a consistent response for a 254-nm-UV-irradiation. All three samples - Cr-0.025%, Cr-0.05%, and Cr-0.1% - exhibit a rapid increase in coloration with increasing dosage. The Cr-0.025% sample also shows sensitivity across a broader range. The smooth curves and stable plateau behavior across the different compositions confirm that this material is responsive and applicable for that analysis.

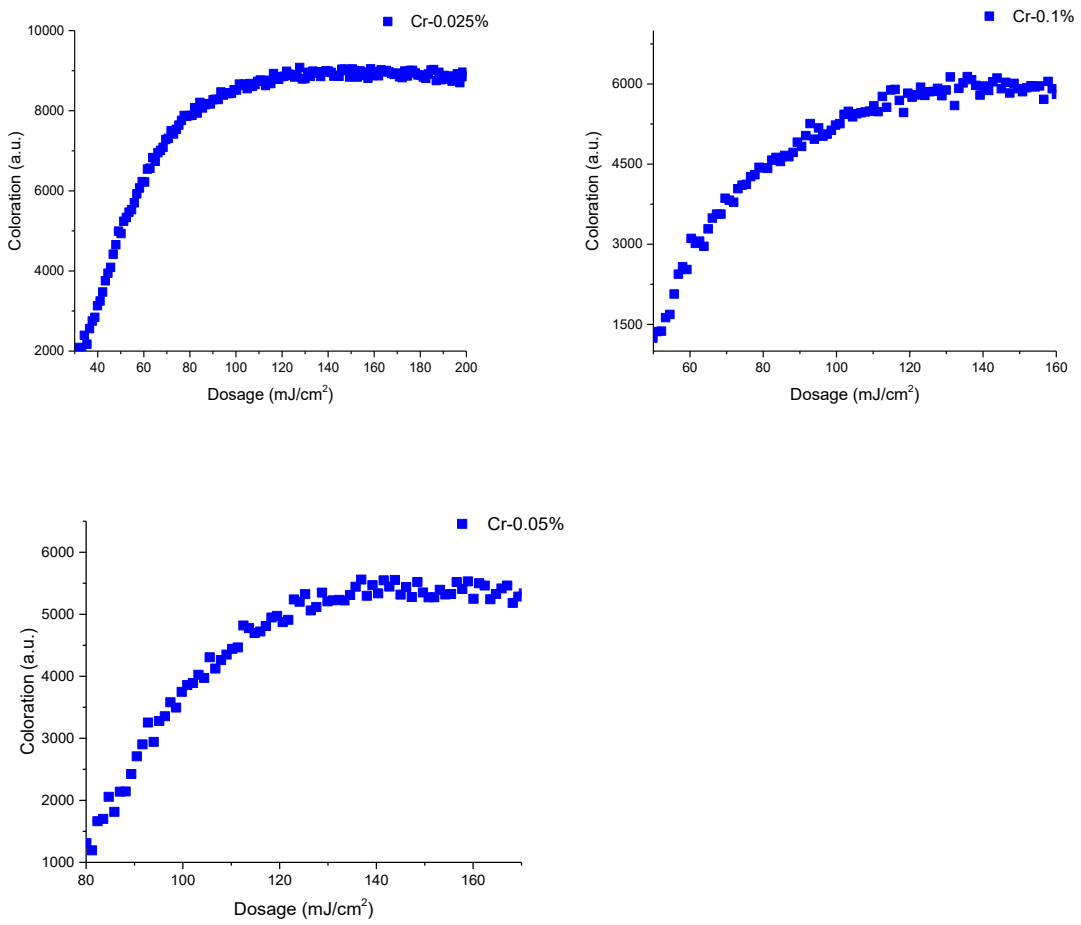

Figure 30. Dose quantification analysis of Cr-doped samples with 254 nm UV light.

Each graph demonstrates a typical saturation curve, with a rapid initial increase followed by a gradual plateau. Among them, the Mn-0.025% and Mn-0.05% samples offer smoother transitions and slightly broader dynamic ranges, while Mn-0.1% shows higher sensitivity in the lower dosage region. The Mn-0.05% sample is not completely saturated in the monitored dose range and has better coloration compared to the other samples within the 254 nm excitation wavelength range. Overall, those samples show dose-responsive behavior to 254 nm UV light, which making them applicable for dose quantification analyses (Fig.31).

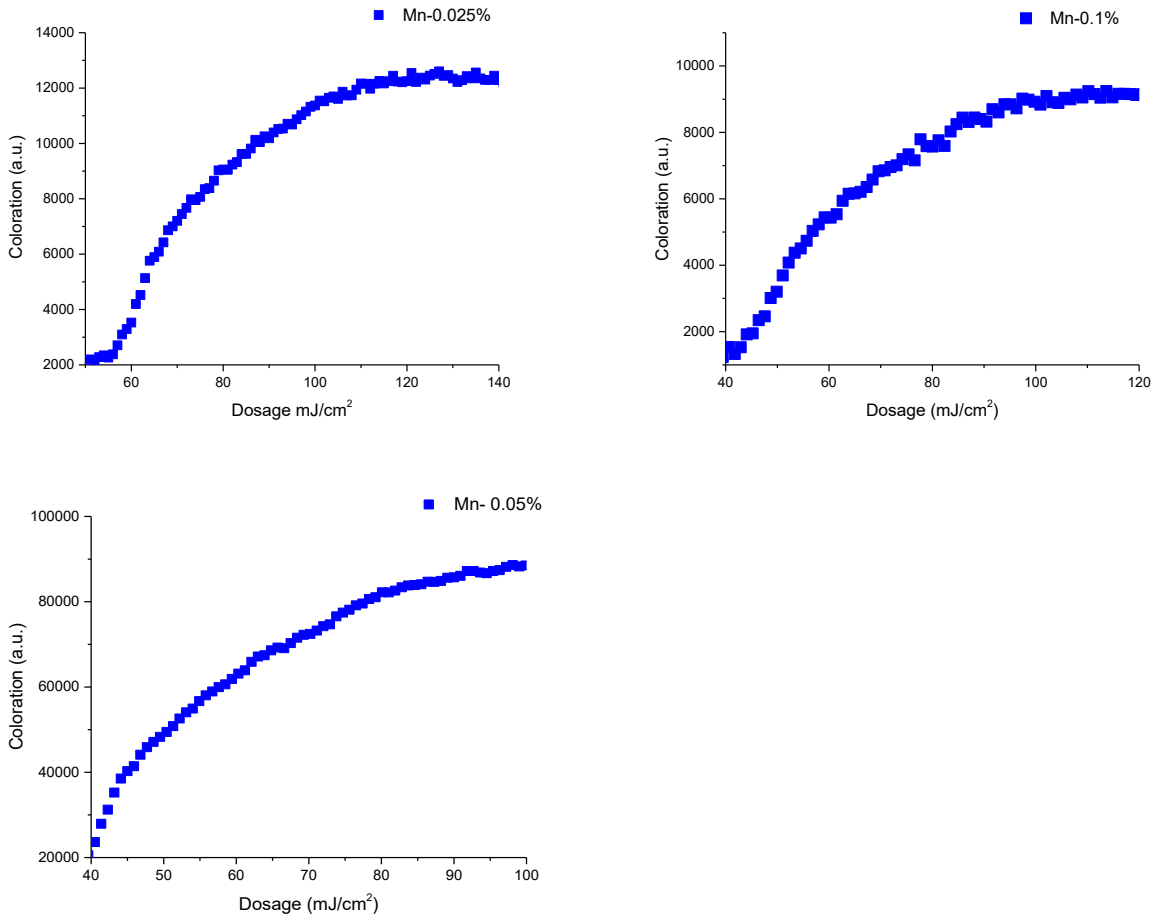

Figure 31. Dose quantification analysis of Mn-doped samples with 254 nm UV light.

3.1.6.2. 302 nm analyses

Figure 32 represents the samples that exhibit a dose-dependent coloration response under 302 nm UV exposure. Each graph follows a characteristic saturation trend, with an initial rapid rise in coloration followed by a plateau. The Fe-0.025% sample demonstrates a more extended dosage range (up to 300 mJ/cm^2), while the Fe-0.1% sample shows higher sensitivity at lower dosages. The consistent and repeatable responses across all concentrations indicate the potential use of these for UV-related applications.

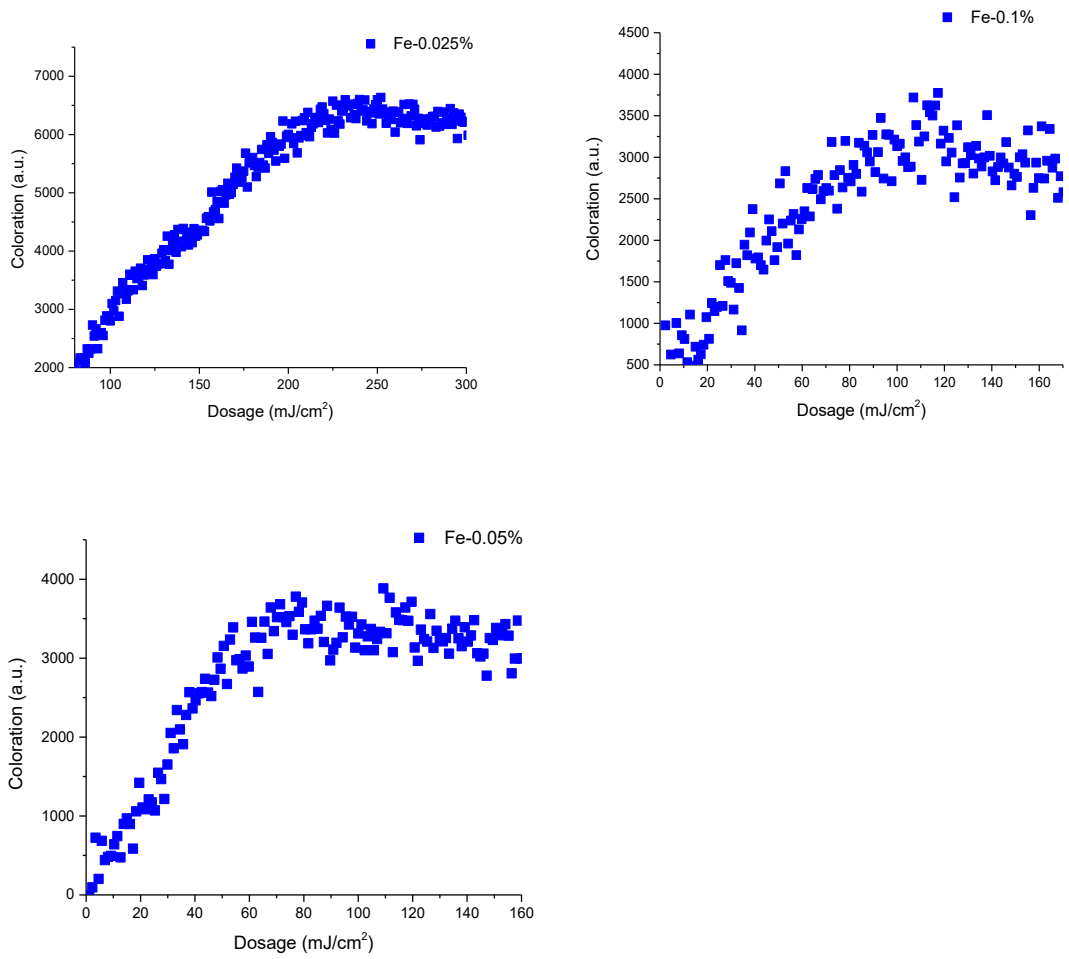

Figure 32. Dose quantification analysis of Fe-doped samples with 302 nm UV light.

The Co-doped samples also demonstrate a dose-dependent coloration response to 302 nm UV light. Each sample shows a well-defined coloration response to UV light with a gradual plateau. The Co-0.025% sample shows a broader dynamic change (up to 300 mJ/cm^2) while others show an intermediate response with a smooth transition (0-160 mJ/cm^2) (Fig.33).

The consistent and reproducible trends across all concentrations confirm the suitability of Co-doped materials for UV dosimetry, but it also depends on the concentration of dopant.

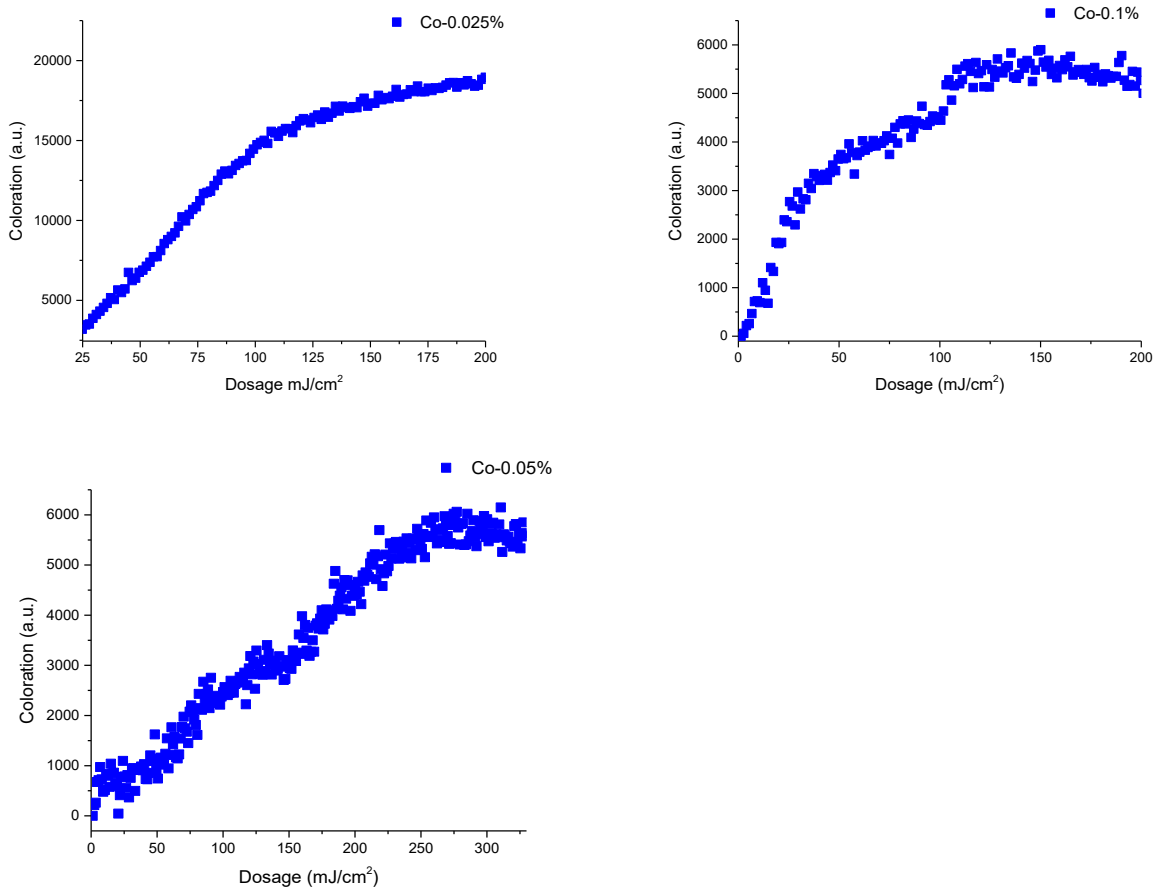

Figure 33. Dose quantification analysis of Co-doped samples with 302 nm UV light.

All graphs show a gradual plateau. Those Cr-doped samples with 302 nm UV light also show light-responsive coloration. The Cr-0.025% sample shows sensitivity in the low dosage range. Cr-0.05% sample displays the same sensitivity but in the low dosage range (<100 mJ/cm^2). Cr-0.1% shows the most promising results with a high dosage range up to 1200 mJ/cm^2, suggesting its applicability for high-dose UV radiation detection (Fig.34).

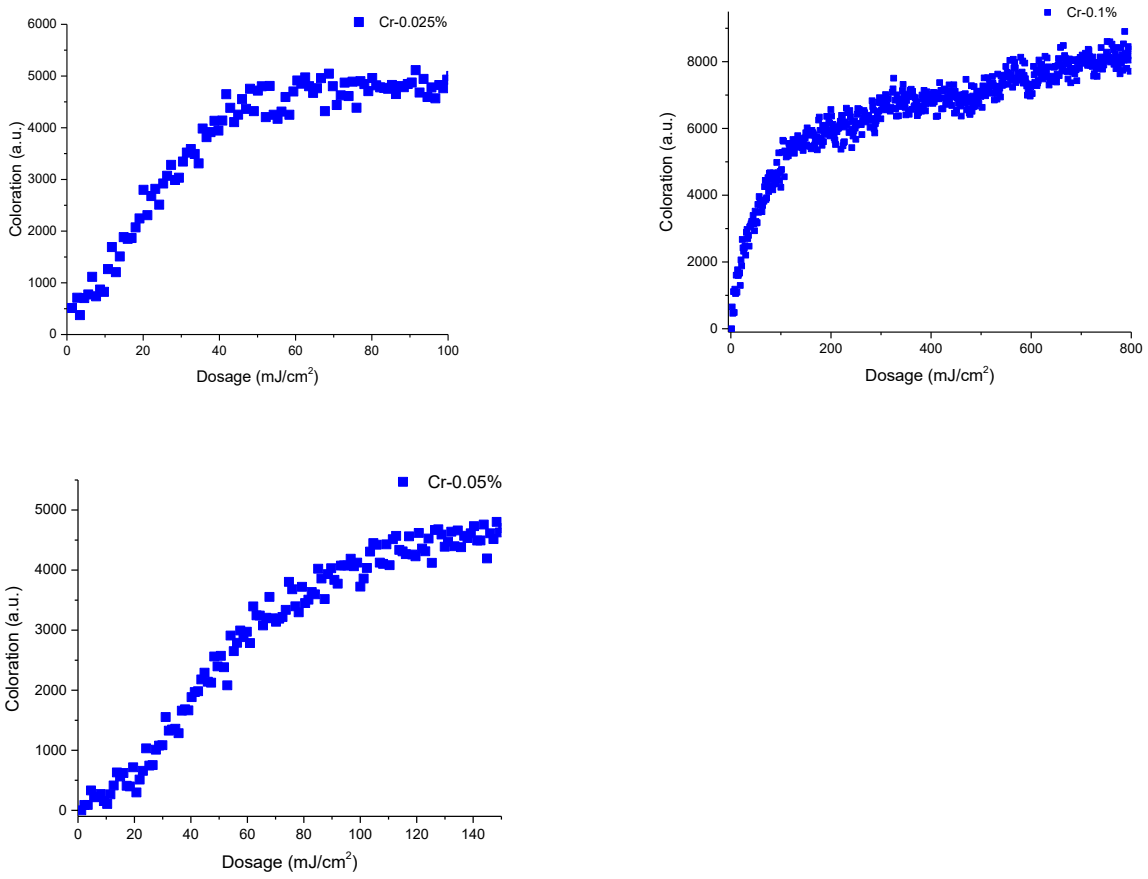

Figure 34. Dose quantification analysis of Cr-doped samples with 302 nm UV light.

Figure 35 represents that the Mn-doped samples are dose-dependent when exposed to 302 nm UV radiation. The Mn 0.025% sample exhibits progressive coloration over a 40-160 mJ/cm² dosage range. The range for the Mn 0.05% sample is even wider, from very low (0 mJ/cm²) to high dosages (1000 mJ/cm²), and therefore is highly suitable for a broad spectrum of UV-related measurements. The 0.1% Mn sample has the same features as the 0.025% sample but with greater sensitivity over the mid-range dosage level (40-160 mJ/cm²). That both different levels of doping are consistent with these response behaviors attests well to the fact that Mn-doped materials are designed for particular UV detection applications.

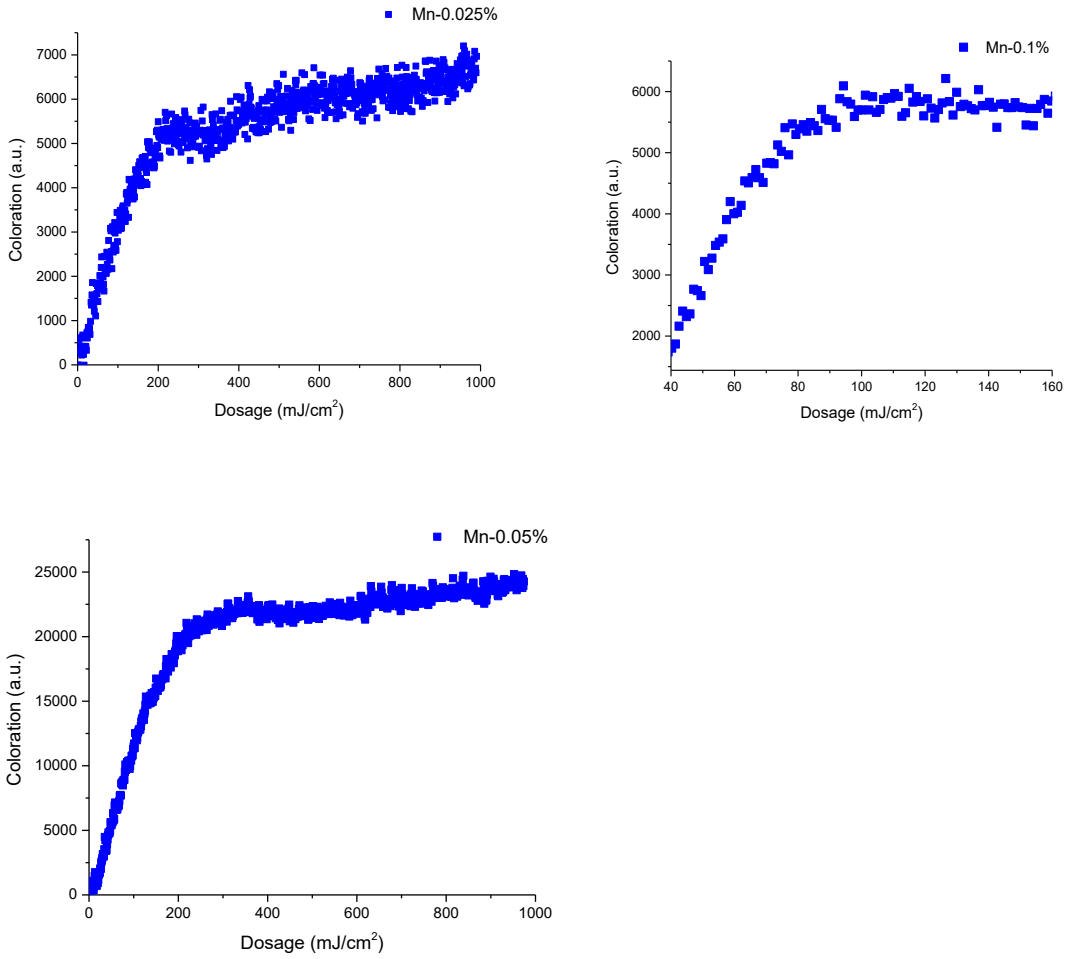

Figure 35. Dose quantification analysis of Mn-doped samples with 302 nm UV light.

3.1.6.3. 365 nm analyses

The Fe-doped samples, Fe-0.025%, Fe-0.05%, and Fe-0.1%, show much weaker photochromic response under 365 nm UV irradiation compared to their performance at 254 nm and 302 nm wavelengths. The Fe-0.025% sample shows very little color change even at high dosages of up to 600 mJ/cm², and the Fe-0.1% samples show only small responses in narrow ranges of dosages (0-80 mJ/cm² and 0-200 mJ/cm²). Most notably missing is the representative saturation curve at shorter wavelengths since all concentrations failed to attain significant coloration intensity. This drastic difference validates that Fe-doped materials are extremely wavelength-dependent in

sensitivity, with good response to 254 nm and 302 nm radiation but effectively no activity at 365 nm. The results categorically demonstrate that these materials are not very suitable for near-UV dosimetry applications. The wavelength-dependent behavior serves to highlight the importance of material choice in relation to the target UV spectrum for accurate dosimetric applications (Fig.36).

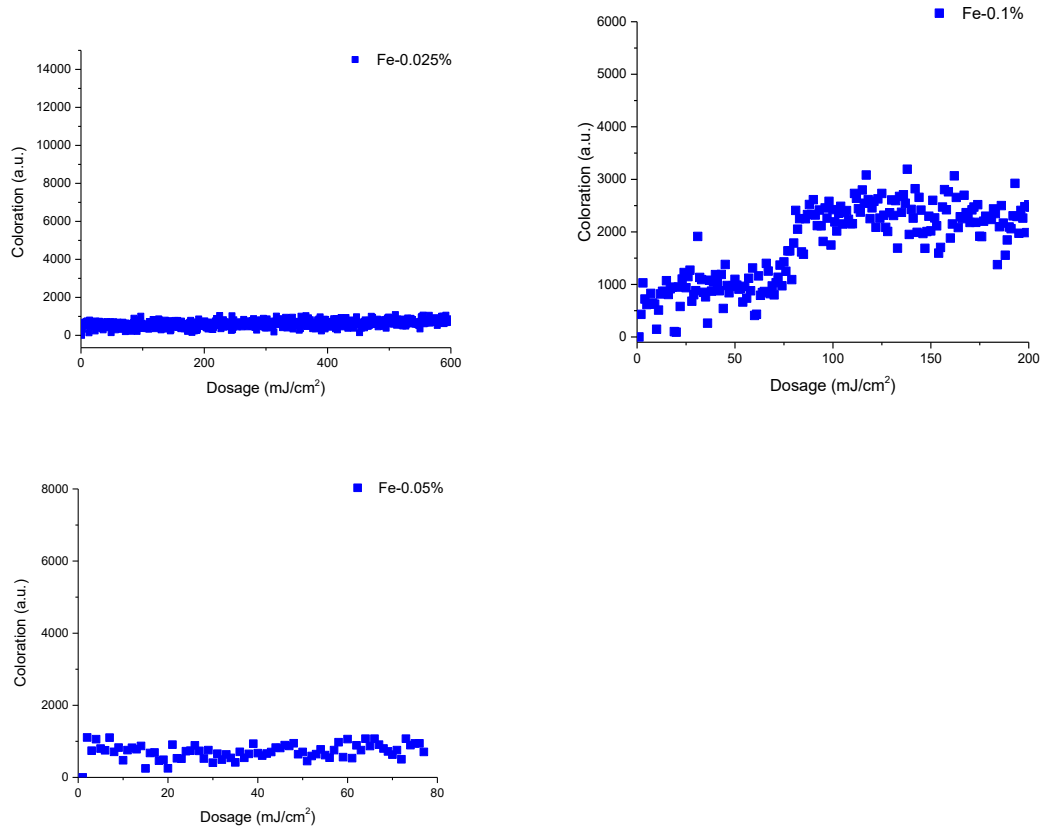

Figure 36. Dose quantification analysis of Fe-doped samples with 365 nm UV light.

In Figure 37, the samples show weaker responses compared to their performance at shorter UV wavelengths (254 nm and 302 nm). These results can be an indicator that Co-doped materials maintain some photosensitivity in the 355-365 nm range; their performance is significantly reduced compared to shorter UV wavelengths, making them less ideal for dosimetry in this UV region. The concentration-dependent variation in response thresholds highlights the need for careful material optimization when targeting near-UV applications.

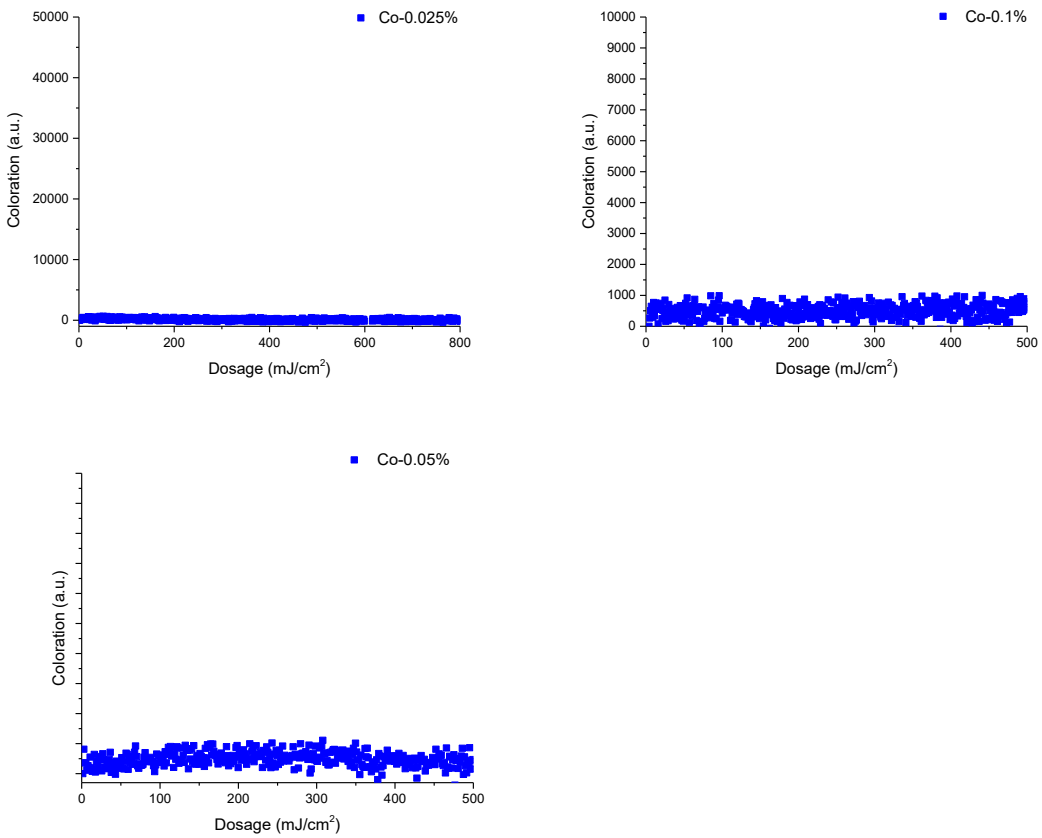

Figure 37. Dose quantification analysis of Co-doped samples with 365 nm UV light.

While all concentrations follow the expected trend of increasing coloration with dosage, their responses at 365 nm appear weaker compared to shorter UV wavelengths (254 nm and 302 nm), where Cr-doped materials typically show more pronounced effects. The absence of clear saturation in these curves suggests the photochromic process remains incomplete within the tested ranges.

According to the results, Cr-doped materials maintain measurable photosensitivity at 365 nm, but with reduced efficiency compared to their performance in shorter-wavelength UV regions (Fig.38).

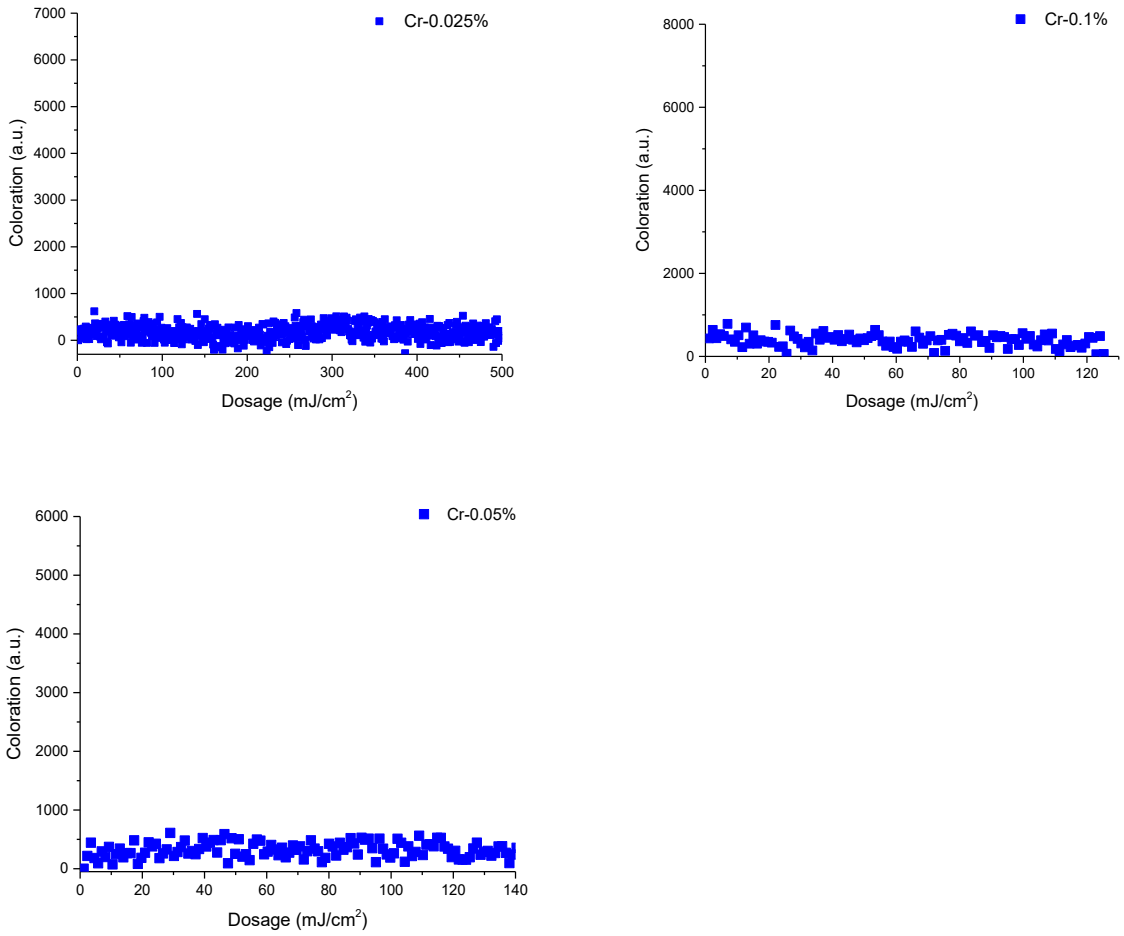

Figure 38. Dose quantification analysis of Cr-doped samples with 365 nm UV light.

None of the Mn-doped samples achieves the pronounced coloration or clear saturation behavior as observed at shorter UV wavelengths (254 nm or 302 nm). The responses remain linear and subdued across all tested dosages and show inefficient photochromic activation at 365 nm.

The minimal and non-saturating responses at 365 nm reinforce the importance of wavelength-specific material selection for accurate UV monitoring applications. For reliable dosimetry, these photochromic materials should be reserved for UVC and UVB detection, where they exhibit stronger, more characteristic photochromic behavior (Fig.39).

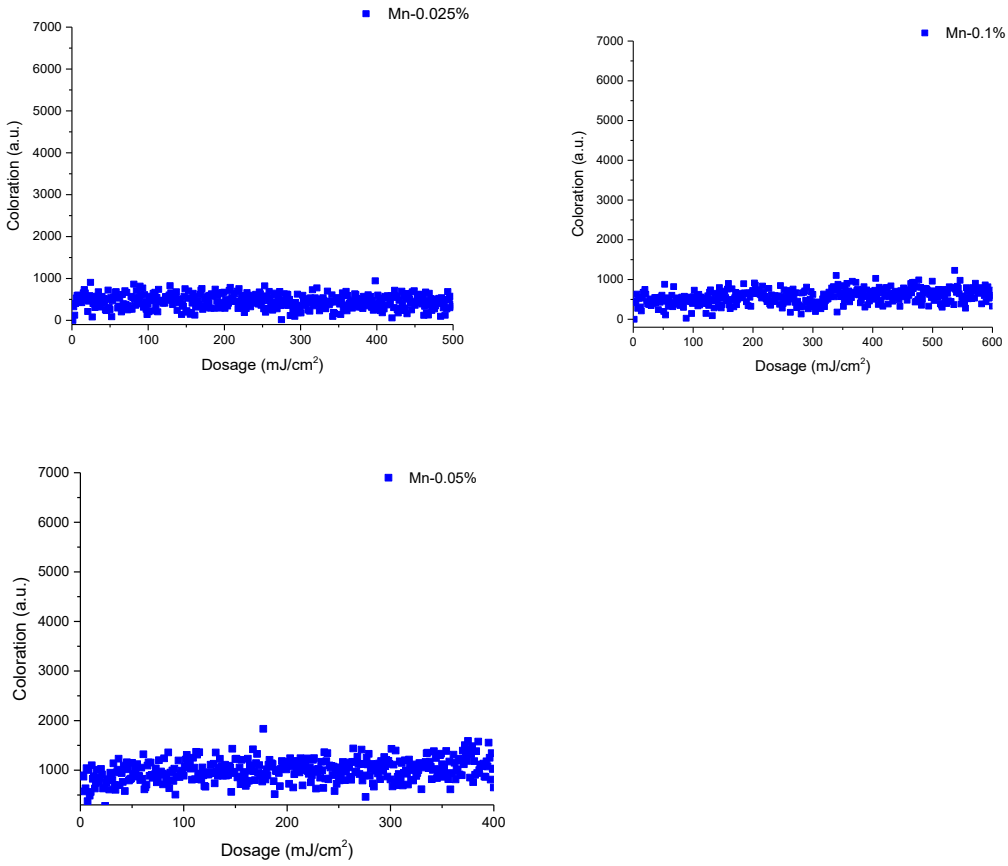

Figure 39. Dose quantification analysis of Mn-doped samples with 365 nm UV light.

3.1.7. Optical microscopy and Luminescence spectroscopy of Eu-0.05% sample

Optical microscopy and luminescence analysis were conducted on the Eu-doped sample to evaluate the reduction process. The emission spectrum around 400-500 nm shows peaks for a combination of Eu^{2+} and Eu^{3+} (sharp lines at 592 nm, 620 nm, 670 nm, and 720 nm, corresponding to $^5D_0 \rightarrow {}^7F_J$ transitions).

The excitation wavelengths (254 nm, 302 nm, 365 nm) can indicate that both valence states are being excited, confirming the coexistence of Eu^{2+} and Eu^{3+} in the sample. The incomplete reduction can be an indicator of the presence of Eu^{3+} emissions. Further optimization of reduction conditions (e.g., temperature, atmosphere, duration) may be required to achieve full conversion to Eu^{2+} if desired (Fig.40).

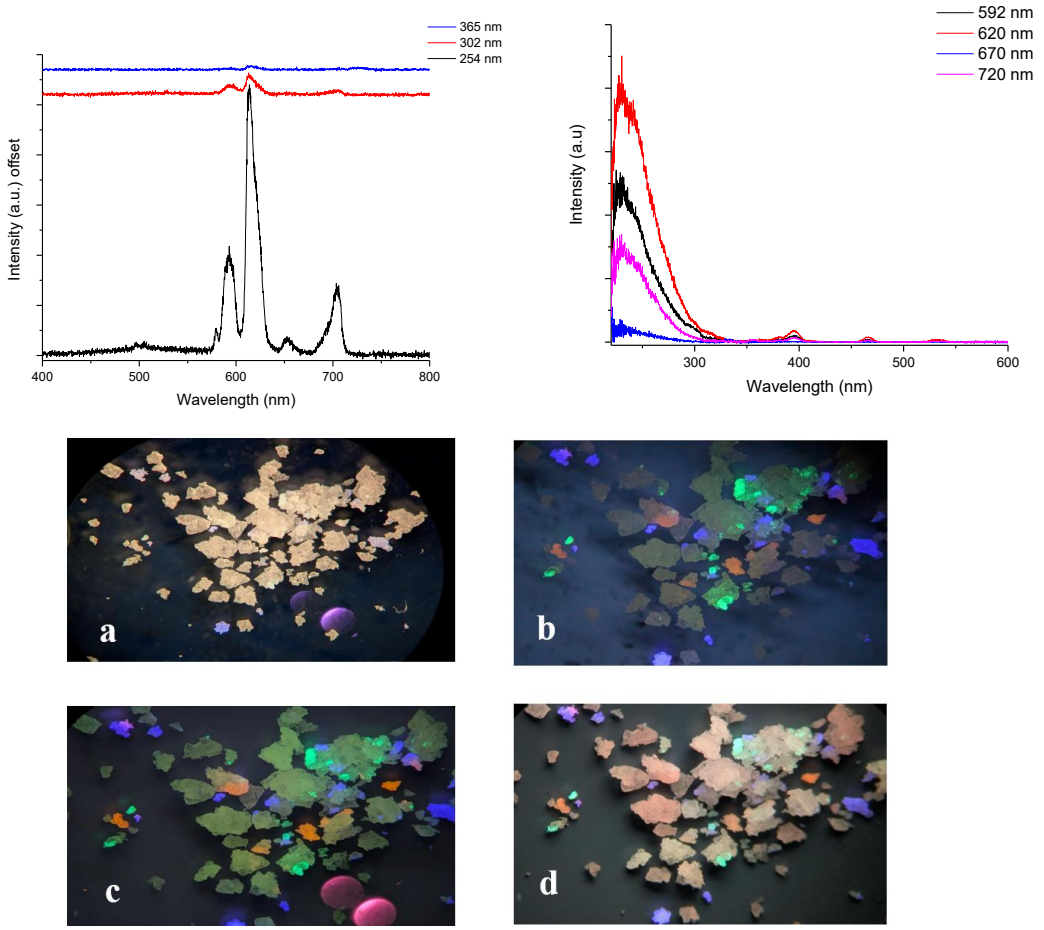

Figure 40. Emission (top left) and excitation (top right) spectra of the Eu-0.05% doped sample with different excitation and emission wavelengths, respectively. Optical microscopy of Eu-doped sample pictures: a) visible light; b) 365 nm; c) 302nm; d) 254 nm.

CONCLUSION

In this work, different dopants were tested with air and reducing atmosphere synthesizing conditions to observe their effect on the photochromic and dosimetric properties of BMS. The study aimed to establish which dopant exhibits the most desirable properties to be used in X-ray and UV applications. Mn, Fe, Cr, and Co were chosen as promising dopant materials for further study. Synthesis conditions were very important in determining the effectiveness of doped materials. Lanthanides (Eu and Dy) were also tested, but they proved to be less promising than transition metals in enhancing photochromism.

The synthesised and prepared samples in the reducing environment showed much better photochromic and responsive properties compared to the samples prepared in air due to the oxygen vacancies. Air-synthesized samples did not meet the desired performance, as they did not show the same intensity and stability of color change, because oxygen vacancy is a crucial point for creating color centers, and there is no oxygen vacancy when the sample is synthesized under air conditions. Their behavior towards radiation exposure was unstable and did not meet the goals of this research. This underscores the need for controlled synthesis conditions to design the properties of BMS-based dosimetric materials. Following the identification of the most promising dopants, additional research was carried out to optimize their concentration within the BMS matrix. The concentration-dependent study identified the optimal dopant concentrations for each sample with stable color changes.

In addition, the wavelength-dependent response of BMS in the UV region makes it particularly attractive for UV dose quantification and monitoring applications. The results point towards the big potential of BMS as a dosimetric material for X-ray, UV, and visible radiation detection. This performance is anticipated to investigate further research activities aimed at the formulation of next-generation photochromic dosimeters. Although the general utility of various dopants for the photochromic purpose, the Fe-doped BMS sample offered comparatively better results regarding color change intensity, stability, and usability across all the samples. The measurements indicated that Fe doping produced the most reproducible and clear photochromic transitions and was thus the most promising candidate for practical dosimetry. The improved response of Fe-doped BMS shows its use as a stable material for radiation detection and monitoring.

The Eu-doped sample displays PeL when excited at 254, 302, and 365 nm, where 254 nm displays the most prominent and highest emission response. This strong and stable luminescence upon short-wavelength UV indicates the prospect of lanthanide-doped samples in luminescent devices. In photochromic behavior, nevertheless, lanthanides lack behind transition metals, whose color changes more intensely and reversibly on irradiation. Moreover, reduction is not a completed process in the Eu-doped sample, indicating an incapacity of existing processing conditions and a possibility for enhancement in future studies regarding optimizing its redox capability and photosensitivity.

One potential future direction is researching photochromic switching in doped BMS samples, which helps us to understand the reliability and stability of these materials under repeated photochromic cycling.

In summary, the research gives an elaborate description of photochromism in doped BMS materials and how they are applied in dose quantification analysis, what dopant material, and the concentration is the best for photochromism enhancement. The research adds to the continuous improvement of efficient and sensitive material for radiation detection. Optimization of the doping process, long-term stability with various dopants, and applications of the materials under real conditions of radiation monitoring can be researched in future work.

Acknowledgements

I would like to express my appreciation to all the individuals who helped me along the way. I am particularly grateful to Mika, whose mentorship gave me the great opportunity to go through varied and challenging experiences in my two-year lab period. I am also highly thankful to Anssi, Sami, and Minnea for continuously helping and supporting me in both of my lab projects.

My personal thanks to my special friends and lab colleagues—Josh, Natalia, Pinja, Cecilia, and Bettiina. Your understanding, support, and assistance in different areas of my life, academic as well as personal, have been of immense importance to me.

To each of you, thank you for being a part of this chapter in my life. It was great to share such a positive experience with IMC!

List of References

1. Zhang, C.; Lin, J. Defect-Related Luminescent Materials: Synthesis, Emission Properties and Applications. *Chem. Soc. Rev.* (**2012**), *41* (23), 7938–7961. doi.org/10.1039/C2CS35215J.

2. Mesaros, A. Luminescent Materials: Synthesis, Characterization and Application. *Appl. Sci.* (**2023**), *13* (20), 11221. doi.org/10.3390/app132011221.

3. Yang, Z.; Hu, J.; Van der Heggen, D.; Jiao, M.; Feng, A.; Vrielinck, H.; Smet, P. F.; Poelman, D. A Versatile Photochromic Dosimeter Enabling Detection of X-Ray, Ultraviolet, and Visible Photons. *Laser Photonics Rev.* (**2023**), *17* (5), 2200809. doi.org/10.1002/lpor.202200809.

4. *Luminescence - Phosphor, Chemistry, Materials | Britannica*. Encyclopedia Britannica. https://www.britannica.com/science/luminescence (accessed 2024-12-03).

5. Sudhakar, P.; Gobi, N.; Senthilkumar, M. 13 - Camouflage Fabrics for Military Protective Clothing. In *Military Textiles*; Wilusz, E., Ed.; Woodhead Publishing Series in Textiles; Woodhead Publishing**, (2008),** 293–318. https://doi.org/10.1533/9781845694517.2.293

6. Du, J.; Yang, Z.; Lin, H.; Poelman, D. Inorganic Photochromic Materials: Recent Advances, Mechanism, and Emerging Applications. *Responsive Mater.* (**2024**), *2* (2), e20240004. https://doi.org/10.1002/rpm.20240004

7. Zhang, J.; Zou, Q.; Tian, H. Photochromic Materials: More Than Meets The Eye. *Adv. Mater.* (**2013**), *25* (3), 378–399. https://doi.org/10.1002/adma.201201521

8. Credi, A. (**2007**). Molecules that make decisions. *Angewandte Chemie International Edition, 46*(29), 5472–5475. https://doi.org/10.1002/anie.200700879

9. Gust, D., Andréasson, J., Pischel, U., Moore, T. A., & Moore, A. L. (**2012**). Data and signal processing using photochromic molecules. *Chem. Commun., 48*(15), 1947–1957. https://doi.org/10.1039/C1CC15329C

10. Kawata, S.; Kawata, Y. "Three-Dimensional Optical Data Storage Using Photochromic Materials." *Chemical Reviews* (**2000**), *100* (5), 1777–1788 https://doi.org/10.1021/cr980073p

11. Bléger, D., & Hecht, S. (**2015**). Visible-light-activated molecular switches. *Angewandte Chemie International Edition*, *54*(39), 11338–11349. https://doi.org/10.1002/anie.201500628

12. Areephong, J., Browne, W. R., Katsonis, N., & Feringa, B. L. (**2006**). Photo- and electrochromism of diarylethene modified ITO electrodes—towards molecular based read–write–erase

information storage. *Chemical Communications*, (37), 3930–3932. https://doi.org/10.1039/b608502d

13. Zacharias, P., Gather, M. C., Köhnen, A., Rehmann, N., & Meerholz, K. (**2009**). Photoprogrammable Organic Light-Emitting Diodes. *Angewandte Chemie International Edition, 48*(22), 4038–4041. https://doi.org/10.1002/anie.200805969

14. **Li, C., & Qi, L.** (2008). Bioinspired fabrication of 3D ordered macroporous single crystals of calcite from a transient amorphous phase. *Angewandte Chemie International Edition, 47*(13), 2388–2393. https://doi.org/10.1002/anie.200705403

15. Munson, C. A., Gottfried, J. L., De Lucia, F. C., McNesby, K. L., & Miziolek, A. W. (**2007**). Laser-based detection methods of explosives. In J. Yinon (Ed.), *Counterterrorist detection techniques of explosives,* 279–321. Elsevier Science B.V. https://doi.org/10.1016/B978-044452204-7/50029-8 .

16. Mehare, M. D., Mehare, C. M., Swart, H. C., & Dhoble, S. J. (**2023**). Recent development in color-tunable phosphors: A review. *Progress in Materials Science,* 133, 101067. https://doi.org/10.1016/j.pmatsci.2022.101067

17. Soni, A. K., & Singh, B. P. (**2020**). Luminescent materials in lighting, display, solar cell, sensing, and biomedical applications. In *Luminescence - OLED Technology and Applications* 1–23. IntechOpen. https://doi.org/10.5772/intechopen.82123

18. Azorín Nieto, J. (**2016**). Present status and future trends in the development of thermoluminescent materials. *Applied Radiation and Isotopes,* 117, 135–142. https://doi.org/10.1016/j.apradiso.2015.11.111

19. Zhu, Y., Sun, H., Jia, Q., Guan, L., Peng, D., Zhang, Q., & Hao, X. (**2021**). Site-Selective Occupancy of Eu^{2+} toward High Luminescence Switching Contrast in $BaMgSiO_4$-Based Photochromic Materials. *Advanced Optical Materials*, *9*(6), 2001626. https://doi.org/10.1002/adom.202001626

20. Ullah, A. Z., Azam, S., Aamer, M., Guo, X., Khan, W., Rahaman, M., Jawad, M., & Ahmad, H. (**2024**). Effect of Eu Concentration on the Optical Properties of $BaMgSiO_4$ Long Persisting Phosphorous Material. *Silicon, 16*(10), 4389–4396. https://doi.org/10.1007/s12633-024-02957-2

21. Bechinger, C., Oefinger, G., Herminghaus, S., & Leiderer, P. (**1993**). On the fundamental role of oxygen for the photochromic effect of WO_3. *Journal of Applied Physics, 74*(7), 4527–4533. https://doi.org/10.1063/1.354370

22. Akiyama, M., Yamada, H., & Sakai, K. (**2011**). Photochromism enhancement in reduced tridymite $BaMgSiO_4$ by Fe-doping. *Journal of the Ceramic Society of Japan, 119*(1389), 338–341. https://doi.org/10.2109/jcersj2.119.338

23. Liu, B., & Barbier, J. (1993). Structures of the stuffed tridymite derivatives, $BaMSiO_4$ (M = Co, Zn, Mg). *Journal of Solid State Chemistry*, *102*(1), 115–125. https://doi.org/10.1006/jssc.1993.1013

24. Zulkafli, N. M. A., Yaakob, M. K., Ridzwan, M. H., Kasim, M. F., Mahat, M. M., Rajmi, R., Mamat, M. H., Mohamad, A. A., & Yahya, M. Z. A. (**2023**). Insight into the role of atomic interaction and ionic radius in Al doped $BiFeO_3$: Structural, electronic, and optical properties. *Physica B: Condensed Matter, 648*, 414417. https://doi.org/10.1016/j.physb.2022.414417

25. Dai, W. B., Huang, K., Fan, Y. M., Li, H., & Xu, M. (**2020**). Structure, valence change, and optical properties of $BaMgSiO_4$:Eu phosphor. *Journal of Luminescence,* 222, 117137. https://doi.org/10.1016/j.jlumin.2020.117137

26. Dai, W. B., Lei, Y. F., Yu, T., Peng, M. Y., & Zhang, Q. Y. (**2015**). Luminescence properties and a substitution defect model for self-reduction of europium ions in silicate Ba(Eu)$MgSiO_4$ phosphors. *Materials Research Bulletin,* 67, 176–184. https://doi.org/10.1016/j.materresbull.2015.03.004

27. Irie, M. (**2000**). Diarylethenes for Memories and Switches. *Chemical Reviews, 100*(5), 1685–1716. https://doi.org/10.1021/cr980069d

28. Van der Heggen, D., Zilenaite, R., Ezerskyte, E., Fritz, V., Korthout, K., Vandenberghe, D., De Grave, J., Garrevoet, J., Vincze, L., Poelman, D., Joos, J. J., & Smet, P. F. (**2022**). A Standalone, Battery-Free Light Dosimeter for Ultraviolet to Infrared Light. *Advanced Functional Materials, 32*(14), 2109635. https://doi.org/10.1002/adfm.202109635

29. Yang, Z., Hu, J., Van der Heggen, D., Feng, A., Hu, H., Vrielinck, H., Smet, P. F., & Poelman, D. (**2022**). Realizing simultaneous X-ray imaging and dosimetry using phosphor-based detectors

with high memory stability and convenient readout process. *Advanced Functional Materials, 32*(31), 2201684. https://doi.org/10.1002/adfm.202201684

30. Lyu, T., Dorenbos, P., Li, C., & Wei, Z. (**2022**). Wide range X-ray to infrared photon detection and energy storage in $LiTaO_3:Bi^{3+},Dy^{3+}$ perovskite. *Laser & Photonics Reviews*, *16*(9), 2200055. https://doi.org/10.1002/lpor.202200055

31. Wang, J., Jeevarathinam, A. S., Jhunjhunwala, A., Ren, H., Lemaster, J., Luo, Y., Fenning, D. P., Fullerton, E. E., & Jokerst, J. V. (**2018**). A wearable colorimetric dosimeter to monitor sunlight exposure. *Advanced Materials Technologies*, *3*(6), 1800037. https://doi.org/10.1002/admt.201800037

32. Smith, A. T., Ding, H., Gorski, A., Zhang, M., Gitman, P. A., Park, C., Hao, Z., Jiang, Y., Williams, B. L., Zeng, S., Kokkula, A., Yu, Q., Ding, G., Zeng, H., & Sun, L. (**2020**). Multi-color reversible photochromisms via tunable light-dependent responses. *Matter, 2*(3), 680–696. https://doi.org/10.1016/j.matt.2019.12.006

33. Chen, J.-K., Shirahata, N., & Sun, H.-T. (**2021**). Metal-free scintillators excite X-ray community. *Nature Photonics, 15*(3), 171–172. https://doi.org/10.1038/s41566-020-00751-1

34. Chen, Q., Wu, J., Ou, X., Huang, B., Almutlaq, J., Zhumekenov, A. A., Guan, X., Han, S., Liang, L., Yi, Z., Li, J., Xie, X., Wang, Y., Li, Y., Fan, D., Teh, D. B. L., All, A. H., Mohammed, O. F., Bakr, O. M., Wu, T., Bettinelli, M., Yang, H., Huang, W., & Liu, X. (**2018**). All-inorganic perovskite nanocrystal scintillators. *Nature,* 561, 88–93. https://doi.org/10.1038/s41586-018-0451-1

35. Shrestha, S., Chen, H., Tedde, S. F., Schmidt, O., Hock, R., Ruehrig, M., Goeken, M., Heiss, W., Anton, G., Brabec, C. J., Fischer, R., Matt, G. J., Feldner, P., Michel, T., Osvet, A., Levchuk, I., Merle, B., & Golkar, S. (**2017**). High-performance direct conversion X-ray detectors based on sintered hybrid lead triiodide perovskite wafers. *Nature Photonics*, *11*(7), 436-+. https://doi.org/10.1038/NPHOTON.2017.94

36. Ou, X., Qin, X., Huang, B., Zan, J., Wu, Q., Hong, Z., Xie, L., Bian, H., Yi, Z., Chen, X., Wu, Y., Song, X., Li, J., Chen, Q., Yang, H., & Liu, X. (**2021**). High-resolution X-ray luminescence extension imaging. *Nature*, 590, 410–415. https://doi.org/10.1038/s41586-021-03251-6

37. Vuori, S., Colinet, P., Norrbo, I., Steininger, R., Saarinen, T., Palonen, H., Paturi, P., Rodrigues, L. C. V., Göttlicher, J., Le Bahers, T., & Lastusaari, M. (**2021**). Detection of X-ray doses with color-changing hackmanites: Mechanism and application. *Advanced Optical Materials, 9*(20), 2100762. https://doi.org/10.1002/adom.202100762

38. Byron, H. C., Swain, C., Paturi, P., Colinet, P., Rullan, R., Halava, V., Le Bahers, T., Lastusaari, M. (**2023**). Highly Tunable Photochromic Sodalites for Dosimetry, Security Marking and Imaging. *Advanced Functional Materials, 33*(42), 2303398. https://doi.org/10.1002/adfm.202303398

39. Holton, W. C., & Blum, H. (**1962**). Paramagnetic Resonance of F-Centers in Alkali Halides. *Physical Review, 125*(1), 89–103. https://doi.org/10.1103/PhysRev.125.89

Appendix

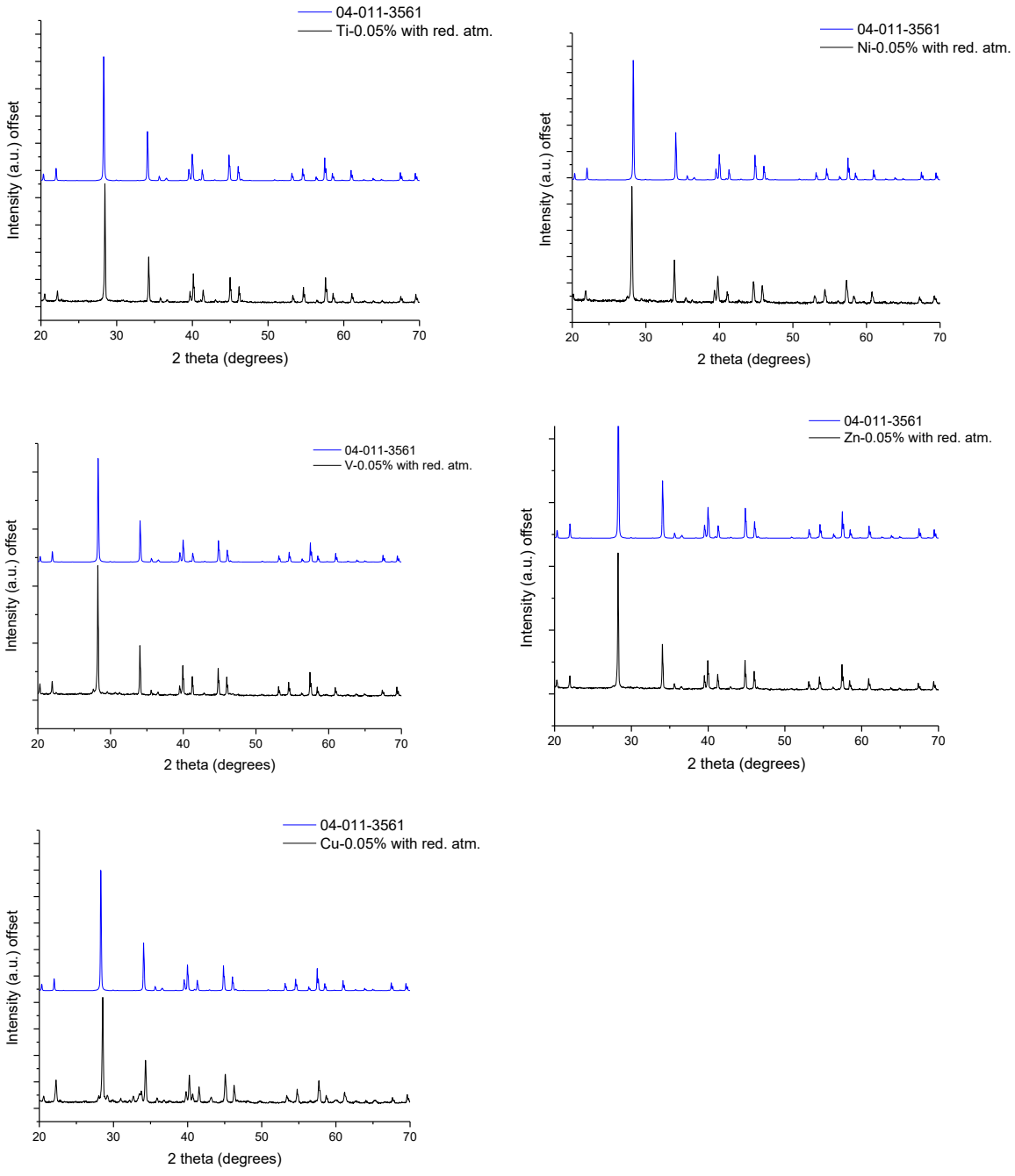

Figure A1. XRD graphs for Transition metal-doped samples under reducing atmosphere were synthesized.

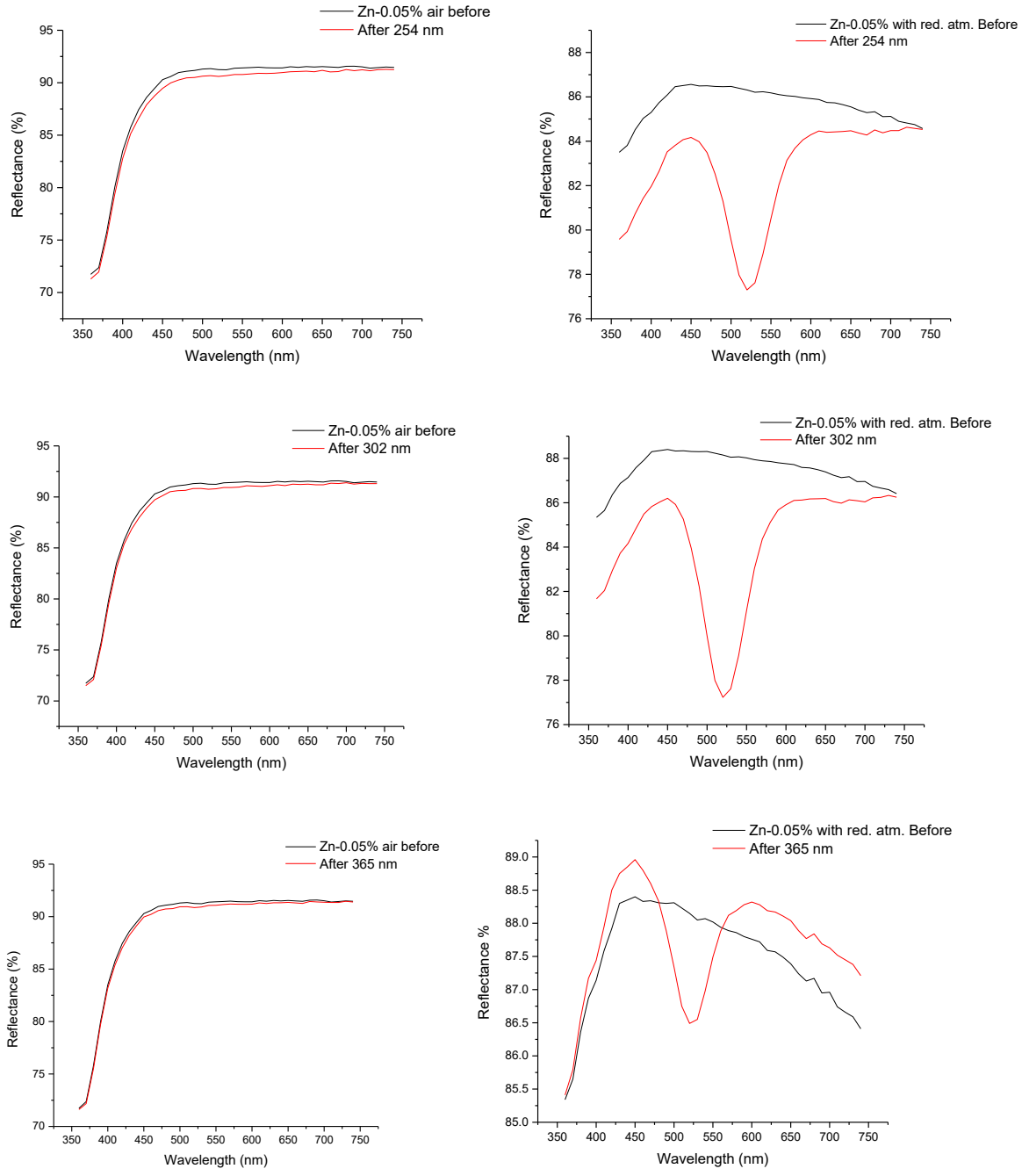

Figure A2. Reflectance Spectroscopy graphs for Zn-doped sample with two different reaction conditions and exposed to three different excitation wavelengths.

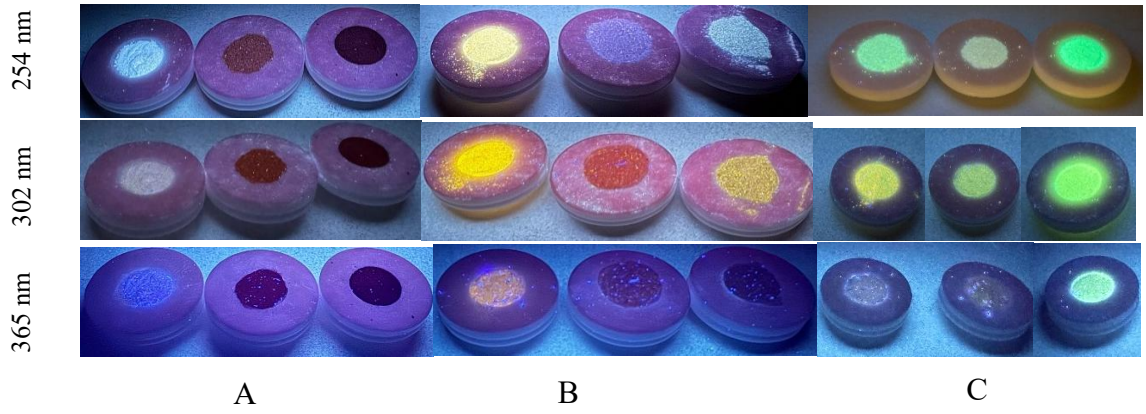

Figure A3: A. Fe-doped samples; B. Cr-doped samples; C. Mn-doped samples with three different concentrations and UV wavelengths.
Concentrations: From left to right for each sample, 0.025%, 0.05%, and 0.1%.

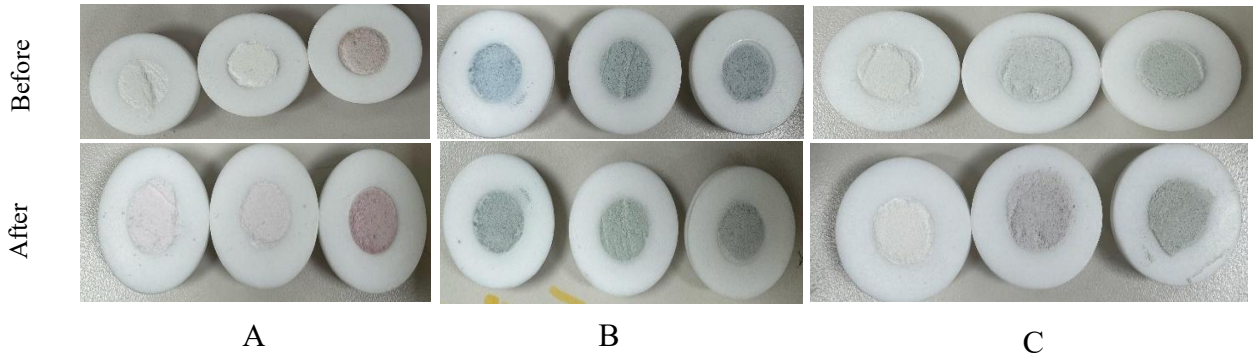

Figure A4. Photochromism observation after 5 minutes of 254 nm UV light exposure
A. Mn-doped samples; B. Co-doped samples; C. Cr-doped samples with three different concentrations.
Concentrations: From left to right for each sample, 0.025%, 0.05%, and 0.1%.